An Exhaustive Multiple Knockout Approach to Understanding Cell Wall Hydrolase Function in *Bacillus subtilis*

Sean A. Wilson[1,2], Raveen K. J. Tank[3,4], Jamie K. Hobbs[3], Simon J. Foster[5], Ethan C. Garner[1,2,*]

[1] Department of Molecular and Cellular Biology, Harvard University, Cambridge, United States.

[2] Center for Systems Biology, Harvard University, Cambridge, United States.

[3] Department of Physics and Astronomy, University of Sheffield, Sheffield, United Kingdom.

[4] Current address: School of Biological Sciences, Faculty of Biology, Medicine and Health, The University of Manchester, Manchester, United Kingdom

[5] School of Biosciences, University of Sheffield, Sheffield, United Kingdom.

Corresponding Author: Ethan C. Garner

NW 445.20, Northwest Building, 52 Oxford Street, Cambridge, MA 02138

*E-mail: egarner@g.harvard.edu

ABSTRACT

Most bacteria are surrounded by their cell wall, containing a highly crosslinked protective envelope of peptidoglycan. To grow, bacteria must continuously remodel their wall, inserting new material and breaking old bonds. Bond cleavage is performed by cell wall hydrolases, allowing the wall to expand. Understanding the functions of individual hydrolases has been impeded by their redundancy: single knockouts usually present no phenotype. We used an exhaustive multiple-knockout approach to determine the minimal set of hydrolases required for growth in Bacillus subtilis. We identified 42

candidate hydrolases. Strikingly, we were able to remove all but two of these genes in a single strain; this "Δ40" strain shows only a mild reduction in growth rate, indicating that none of the 40 hydrolases are necessary for growth. The Δ40 strain does not detectably shed old wall, suggesting that turnover is not essential for growth. The remaining hydrolases in the Δ40 strain are LytE and CwlO, previously shown to be synthetically lethal. Either can be removed in Δ40, indicating that either hydrolase alone is sufficient for cell growth. Screening of environmental conditions and biochemistry revealed that LytE activity is inhibited by Mg2+ and that RlpA-like proteins may stimulate LytE activity. Together, these results suggest that the only essential function of cell wall hydrolases in B. subtilis is to enable cell growth by expanding the wall and that LytE or CwlO alone is sufficient for this function. These experiments introduce the Δ40 strain as a tool to study hydrolase activity and regulation in B. subtilis.

IMPORTANCE

In order to grow, bacterial cells must both create and break down their cell wall. The enzymes that are responsible for these processes are the target of some of our best antibiotics. Our understanding of the proteins that break down the wall – cell wall hydrolases – has been limited by redundancy among the large number of hydrolases many bacteria contain. To solve this problem, we identified 42 cell wall hydrolases in *Bacillus subtilis* and created a strain lacking 40 of them. We show that cells can survive using only a single cell wall hydrolase; this means that to understand the growth of *B. subtilis* in standard laboratory conditions, it is only necessary to study a very limited number of proteins, simplifying the problem substantially. We additionally show that the

46 Δ40 strain is a research tool to characterize hydrolases, using it to identify 3 'helper'
47 hydrolases that act in certain stress conditions.

48 **INTRODUCTION**

49 Most bacterial cells are surrounded by a peptidoglycan (PG) cell wall – a load-
50 bearing structure that protects cells from lysing due to their high internal turgor (1).
51 Bonds must be broken in the PG for cells to expand during growth (2). PG is built from
52 disaccharide subunits linked to stem peptides. As new PG is inserted into the wall, the
53 disaccharides are polymerized into long chains, and their stem peptides are crosslinked
54 into the existing wall (3).

55 The enzymes that break PG bonds are termed cell wall hydrolases (hereafter
56 'hydrolases'). Hydrolases fall into several broad categories with different chemical
57 specificities (4). Amidases cleave the stem peptide from the sugar subunit.
58 Endopeptidases cleave bonds between peptides within the stem peptide. Lytic
59 transglycosylases (LTGs) and lysozymes (both of which are muramidases), cleave
60 between the disaccharide subunits (MurNAc-GlcNAc), reversing the transglycosylase
61 reaction that polymerizes glycan chains. Glucosaminidases target the other bond
62 between sugar subunits (GlcNAc-MurNAc), reversing a cytoplasmic step of PG
63 synthesis. The LTG reaction mechanism is not a hydrolysis reaction; however, to avoid
64 introducing new terminology and to improve readability, we will use the term
65 'hydrolases' generally to refer to all PG cleavage enzymes, including LTGs. A wide
66 array of different protein domains are capable of hydrolase activity – for example, there
67 are at least 7 distinct domains with LTG activity and well over 100 distinct domains with
68 hydrolase activity discovered thus far (5, 6).

69 Hydrolase activity is essential: without the breakage of PG bonds, the cell wall
70 cannot expand to accommodate the accumulating biomass it contains (2). Hydrolases
71 are also involved in a variety of other processes that require modification of the cell wall:
72 turning over old PG, cell separation, and sporulation, conjugation, and motility (4, 7).
73 Perhaps owing to the multiple cellular functions that require hydrolases, many bacteria
74 have a large number of hydrolases. *Bacillus subtilis* and *Escherichia coli,* for example,
75 each contain at least 20 hydrolases (4, 8). The large number of hydrolases in each
76 bacterium, combined with a high degree of functional and enzymatic redundancy
77 between them, has made it difficult to identify specific cellular functions for many
78 hydrolases. Single knockouts rarely present clear phenotypes due to compensation by
79 other hydrolases (4, 9). However, multiple-knockout approaches in *B. subtilis* have been
80 successful in revealing the importance of LytE and CwlO for cell growth, uncovering the
81 role of LytC and LytD in cell wall turnover, and identifying LytE, LytF, and CwlS as cell
82 separation hydrolases (4, 10, 11).
83 *lytE* and *cwlO* had been previously shown to be synthetically lethal when both
84 are deleted in *B. subtilis* (10, 12). The requirement of LytE or CwlO for cell growth was
85 demonstrated via microscopy and genetics: upon depletion of LytE in a *cwlO* null
86 mutant, or vice versa, cell elongation slows and then stops completely before cells lyse
87 (12). To test whether any other hydrolases were essential for *B. subtilis* growth, we
88 employed an exhaustive multiple-knockout approach. We created a minimal hydrolase
89 strain that allows the study of hydrolases in isolation, making it easier to assign
90 functions to uncharacterized hydrolases. Using this multiple hydrolase knockout strain, it
91 is straightforward to assay the biochemical activity and determine the effect of

92 hydrolases alone or in any desired combination on phenotypes like cell width, cell wall
93 turnover, cell growth, or any other process.

94 **RESULTS**

95 **Construction of a multiple hydrolase knockout strain**

96 To identify the minimal set of hydrolases required for growth in *B. subtilis* PY79,
97 we constructed a strain in which we sequentially removed as many hydrolases as
98 possible. We used PHMMER to screen the *B. subtilis* proteome for proteins containing
99 cell wall hydrolase domains present in known hydrolases (4, 5, 8, 13, Table S2). The
100 results of this search are shown in Table 1. Cell wall hydrolases present in *B. subtilis*
101 168 but not present in PY79, our wild-type (WT) background, are included for
102 completeness, though we did not generate knockouts for these. Candidate hydrolases
103 previously shown to be unable to degrade intact PG (indicated in Table 1) were also not
104 knocked out, nor were candidate hydrolases with transmembrane domains, as these
105 are unlikely to be able to reach into the cell wall space far enough to directly participate
106 in growth. We found 56 candidate hydrolases in the initial search (all shown in Table 1);
107 of these, 50 were present in PY79. 4 were excluded due to previous work
108 demonstrating lack of activity against intact PG (AmiE, NagZ, LytB, and PgdS), and 4
109 were excluded due to being membrane-bound (MltG, SweC, SpoIIQ, and SpoIVFA),
110 leaving 42 candidate hydrolases for our study.

111 We next generated single knockouts for each of the candidate hydrolases by
112 replacing the gene with an antibiotic resistance cassette flanked by loxP sites. We then
113 sequentially combined all knockouts into a single strain, using Cre-lox mediated loop
114 outs to remove markers when necessary (Figure 1). After each loop out step, we

115 verified deletion of all modified loci by PCR. After all knockouts had been combined into
116 a single strain, whole-genome sequencing was used to confirm all deletions and to
117 identify any genomic rearrangements or mutations that occurred during the construction
118 process. Despite the multiple rounds of transformation and loop outs this strain was
119 subjected to, with up to 4 resistance cassettes removed simultaneously multiple times,
120 we found no evidence of genomic rearrangements based on read coverage from DNA
121 extracted during exponentially growing cells (Figure S1) (14), and only 8 SNPs leading
122 to 5 point mutations in genes involved in unrelated processes (Table S1).

123 Ultimately, this effort produced a strain lacking 40 hydrolases, which we termed
124 "Δ40". The Δ40 strain is lacking all the identified hydrolases that met our criteria save
125 two - LytE and CwlO, two synthetically lethal endopeptidases previously shown to be
126 essential for growth (10). We were able to further knock out either *lytE* or *cwlO* in the
127 Δ40 strain, but not both, due to their synthetic lethality.

128 **Hydrolase activity is greatly reduced in the Δ40 strain**

129 To assess whether any other unidentified hydrolases remained in the Δ40 strain,
130 we conducted PG profiling of both wild type (WT) cells and the Δ40 strain (15), allowing
131 us to determine the abundance of hydrolase products in their cell walls (Figure 2, Table
132 S3).

133 Our PG profiling assay has limitations: as PG profiling relies on muramidase
134 digestion to yield soluble muropeptides for HPLC analysis, we could not use this assay
135 to detect hydrolases with muramidase activity. Likewise, as D,D-endopeptidases
136 produce products that are indistinguishable from unmodified PG, we cannot

137 unambiguously assign specific PG products to D,D-endopeptidases in these
138 experiments.

139 We compared the relative abundance of different PG hydrolase products in the
140 Δ40 and WT strains (Figure 2B, Table S3). The Δ40 strain showed a very small amount
141 of amidase activity (~20-fold reduction vs WT, 0.8% vs 0.04% of all muropeptides,
142 p=0.0161, unpaired t test) and a reduction of glucosaminidase activity (~2-fold reduction
143 vs WT, 0.8% vs 0.5% of all muropeptides, p=0.0279, unpaired t test), indicating that
144 these classes of hydrolases had been successfully reduced in the Δ40 strain. The
145 residual glucosaminidase activity could represent A) a yet unknown minor
146 glucosaminidase with a novel fold or B) sample degradation during PG purification. We
147 observed no change in D,L-endopeptidase activity in the Δ40 strain (5.2% vs 4.8% of all
148 muropeptides, p=0.4094, unpaired t test), an expected result given Δ40 retains the D,L-
149 endopeptidases LytE and CwlO. In agreement with previous work (15), L,D-
150 endopeptidase activity was not detected in any strain. D,L-endopeptidases cleave
151 between the mDap and iso-D-Glu residues in the stem peptide, while L,D-
152 endopeptidases cleave between iso-D-Glu and L-Ala.

153 Unexpectedly, the Δ40 strain also showed an increase in LTG activity (Figure 2B,
154 ~1.75-fold increase vs WT, 1.4% vs 2.3% of all muropeptides, p=0.0125, unpaired t
155 test). We found that this remaining LTG activity required MltG. Removing *mltG* from the
156 Δ40 strain substantially reduced apparent LTG activity (Figure 2B, ~80-fold reduction vs
157 Δ40, 2.3% vs 0.03% of all muropeptides, p<0.0001, unpaired t test). MltG's catalytic
158 domain is predicted to be extracellular, although MltG is likely too small to reach far
159 enough into the cell wall space to directly participate in cell wall expansion. MltG has

160 been shown to be involved in membrane-proximal PG metabolism, cleaving PG at a
161 specific distance from the membrane to produce 7-dissacharide long glycan strands
162 (16–18).

163 Additionally, we measured the rate of autolysis in the Δ40 strain. Autolysis occurs
164 when hydrolases become dysregulated and degrade the wall in an uncontrolled way,
165 leading to cell lysis. Disruption of the energized membrane via energetic poisons, or
166 treatment with antibiotics can cause autolysis (19). In *B. subtilis*, the hydrolases LytC
167 and LytD are the main effectors of autolysis, with LytE and LytF additionally having
168 smaller effects (7, 20).

169 Δ*cwlO* and Δ*lytE* cells had approximately WT rates of autolysis, with nearly 100%
170 of cells being lysed after 5H of treatment with 75 mM sodium azide or 100 µg/ml
171 ampicillin. In contrast, the Δ40 strain had a significantly slower rate of autolysis in both
172 treatment conditions, with the Δ40 Δ*lytE* strain showing only a ~10% reduction in OD_{600}
173 after 24H of treatment and the Δ40 strain itself showing a ~40% OD_{600} reduction after
174 24H. The nonzero autolysis rate in the Δ40 Δ*lytE* background could imply the
175 involvement of CwlO in autolysis, could represent non-hydrolase-mediated lysis, or
176 could suggest a remaining hydrolase with a minor role in autolysis.

177 **Cell growth and morphology are similar in the Δ40 strain relative to wild type.**

178 We next characterized the growth rate of the Δ40 strain. The Δ40 strain grew
179 slightly slower than WT cells in rich, undefined media (LB), but grew at the same rate as
180 WT cells in both rich, defined media (CH) and fully synthetic media ($S7_{50}$ with glucose
181 and amino acids, see Methods for details) (Figure 3A). This suggests that the activity of
182 LytE and CwlO together are mostly sufficient for normal cell growth, although when

183 pushed towards higher growth rates other cell wall hydrolases may contribute to growth.
184 To investigate the individual effects of LytE and CwlO on the cell growth rate, we made
185 knockouts of *lytE* and *cwlO* in both WT and Δ40 backgrounds. Δ40 Δ*lytE* and Δ40 Δ*cwlO*
186 both exhibited a reduction in growth rate compared to Δ40 which was especially
187 pronounced in LB media. We observed cell lysis in both Δ40 Δ*lytE* and Δ40 Δ*cwlO*
188 strains in phase-contrast images, which could contribute to their slower growth rates as
189 measured in bulk by OD_{600} (Figure 4A). On the other hand, Δ*lytE* or Δ*cwlO* in a WT
190 background had the same growth rate as WT. This suggests either that in WT cells,
191 other hydrolases participate in but are not strictly required for growth, or that LytE and
192 CwlO are not being expressed highly enough to maintain normal growth on their own in
193 the Δ40 background.
194 Next, we quantified cell dimensions in these strains using FM 5-95 membrane
195 stain. Δ40 cells had a WT cell length and were 3% wider (Figure 4B, $p<0.0001$, unpaired
196 t-test with Welch's correction). Δ*cwlO* cells were 13% wider and 18% shorter than WT
197 cells, a phenotype that persisted in the Δ40 Δ*cwlO* strain (Figure 4B, $p<0.0001$ for all
198 comparisons: unpaired t-test with Welch's correction for width comparisons, Mann-
199 Whitney test for length comparisons). Δ40 Δ*cwlO* cells were less able to control their
200 width as compared to Δ40 cells, having a 1.5x wider cell width distribution (Figure 4B,
201 7.5% vs. 11.33% coefficient of variation, F test $p<0.001$). In contrast, Δ*lytE* cells were
202 only slightly wider than WT cells (Figure 4B, 1%, $p<0.0001$, unpaired t-test with Welch's
203 correction), and Δ40 Δ*lytE* cells were slightly narrower (Figure 4B, 1%, $p<0.0001$,
204 unpaired t-test with Welch's correction) than Δ40 strain alone, with a slight decrease in
205 length (Figure 4B, $p<0.0001$, Mann-Whitney test). Thus, CwlO appears to be involved in

206 cell width maintenance, as removing *cwlO* causes changes in cell width both in Δ40 and
207 WT backgrounds, consistent with previous reports (12). Furthermore, given that
208 removing *cwlO* increases the cell width coefficient of variation in the Δ40 background
209 but does not increase the width variation when deleted from WT cells, other hydrolases
210 must also have a role in width homeostasis.

211 We then quantified the chain length for the Δ40 strain and derivatives. Individual
212 B. subtilis cells are often found connected to their siblings via a common cell wall
213 septum as cell separation and cell division do not always occur at the same time in this
214 organism. Cell separation requires the action of hydrolases that cleave between the two
215 connected cells – several different hydrolases serve this purpose in B. subtilis, primarily
216 LytF, CwlS, and LytE (11, 21, 22). In WT cells, the average chain length was
217 comparable to the length of individual cells (Figure 4C, ~4.5 μm per chain vs ~3.5 μm
218 per cell). The maximum chain length observed was 150 μm. Δ*cwlO* and Δ*lytE* mutants
219 had a similar average chain length although the Δ*lytE* mutant had a larger maximum
220 chain length (Figure 4C, 300 μm), consistent with the known role of LytE in cell
221 separation.

222 In contrast, the Δ40 strain had a significant increase in the average chain length
223 (Figure 4C, 120 μm), nearly as long as the longest observed WT chain. The Δ40 Δ*cwlO*
224 strain was similar to the Δ40 strain, while the Δ40 Δ*lytE* strain had a large increase in
225 the average chain length (250 μm), almost double that of the longest observed WT
226 chain. Because the Δ40 Δ*lytE* strain lacks all cell separation hydrolases, the remaining
227 cell separation in this strain was likely due to mechanical tearing of cells under the
228 vigorous shaking conditions needed to be able to measure accurate culture OD_{600} for

229 these experiments; the ends of the chains had visible, phase-light debris resembling
230 torn cells still attached visible by TEM (Figure S3). In gentler culture conditions on a
231 roller drum, this strain grows as a large clump of cells visible to the naked eye.

232 Additionally, we tested the ability of the Δ40 strain to sporulate. Hydrolases are
233 involved in both entry into sporulation, as well as exit from the spore during germination
234 (23–25). We found that the Δ40 was not able to sporulate (Figure 2B, p=0.3859, one
235 sample t test vs efficiency of 0), likely because it lacks SpoIID and SpoIIP, causing a
236 block at the engulfment stage of sporulation (25).

237 **Δ40 cells do not detectably turn over their cell wall**

238 Hydrolases are involved in cell wall turnover, where old PG material is shed from
239 the cell wall (26). We measured the rate of cell wall turnover of both WT and Δ40 cells
240 using pulse-chase labeling with the radioactive cell wall precursor ^{3}H-N-
241 acetylglucosamine (^{3}H-GlcNAc). This revealed that, while WT cells turn over PG at a
242 rate of about 50% per generation in agreement with previous work (26), turnover in Δ40
243 strain was not detectable, with a rate not significantly different from zero (Figure 5A,
244 p=0.4837, one sample t test vs. rate of 0). These results suggests that LytE and CwlO,
245 the only identifiable remaining hydrolases in the Δ40 strain, likely do not contribute to
246 cell wall turnover. Furthermore, this data suggests that cell wall turnover is not an
247 essential process: cell growth only requires the cleavage of bonds so the cell can
248 expand.

249 As hydrolase-deficient mutants have been shown to have altered cell wall
250 thickness (27, 28) we measured the cell wall thickness of the Δ40 strain using
251 transmission electron microscopy (TEM) and atomic force microscopy (AFM). We found

252 that the wall was significantly thicker only in dehydrated samples measured using AFM
253 (Figure 5B, center, p=0.0007, unpaired t test); measurements on TEM images or on
254 hydrated AFM samples showed no significant differences (TEM: Figure 5B, left,
255 p=0.1382, unpaired t test; hydrated AFM: Figure 5B, right, p=0.2887, unpaired t test).
256 The WT cell wall was more uniform in appearance in both TEM and AFM images, while
257 the Δ40 strain had more heterogeneity in density and thickness, in particular on the
258 outer face of the wall, with an increase in the presence of "ruffles" on the outer face of
259 the cell wall in the Δ40 strain (Figure 5C,D). These "ruffles" may represent the additional
260 old cell wall material present due to the strongly reduced turnover rate. The internal face
261 of the cell wall appeared denser than the external face of the wall in both the WT and
262 Δ40 strains (Figure 5D). The internal face of the cell wall in the Δ40 strain appeared to
263 have both a denser meshwork and an increased number of larger pores as compared
264 with the WT strain.

265 Substantial changes to the cell wall ultrastructure occur during sample prep for
266 TEM, especially in the outer layers of the cell wall (29–31); it would be interesting to
267 apply additional, less perturbative EM modalities such as cryo-electron microscopy to
268 the Δ40 strain to help clarify the exact nature of the changes to the Δ40 cell wall. It is
269 possible that both TEM and hydrated AFM highlights mostly the denser, newer cell wall
270 material, while dehydrated AFM allows visualization of all the cell wall, including the
271 more loosely-bound older wall material.

272 **Δ40 Δ*cwlO* cells are sensitive to various stresses, including ionic stress**

273 Although the Δ40 strain grew mostly normally under our standard lab conditions,
274 we wondered whether the absence of so many hydrolases would sensitize cells to

275 stress conditions. We used a spot dilution assay to measure the viability of our strains
276 under a variety of stress conditions: temperature, ionic stress, pH, and osmotic stress
277 (Figure 6). In all conditions, including our control (37˚C), Δ40 cells had fewer CFUs than
278 WT. This is expected because Δ40 cells grow in long chains, and thus cells cannot
279 readily separate into individual CFUs. In all stress conditions Δ40 cells were similarly
280 viable to WT cells, as were Δ*lytE,* Δ*cwlO,* and Δ40 Δ*lytE* cells. However, Δ40 Δ*cwlO*
281 cells were susceptible to multiple stresses, including low pH, low temperature, and ionic
282 stress.

283 We were particularly intrigued by the susceptibility of Δ40 Δ*cwlO* to Mg^{2+}. Mg^{2+} is
284 coordinated between PG and teichoic acids (32), and this Mg^{2+} binding is thought to
285 give structural stability to the cell wall (31, 33). High levels of Mg^{2+} are often protective
286 against cell wall perturbations, including knockouts of hydrolases, PBPs, or components
287 of the Rod complex (10, 34); thus, the Mg^{2+} sensitivity of the Δ40 Δ*cwlO* strain seemed
288 counterintuitive. Our experiments indicated Δ40 Δ*cwlO* cells were sensitive to both Ca^{2+}
289 and Mg^{2+}; growth was inhibited by the addition of 10 mM $MgCl_2$, 10 mM $MgSO_4$, and 10
290 mM $CaCl_2$, but not by the addition of 20 mM NaCl, suggesting that the growth inhibition
291 was not due to changes in ionic strength or chloride ions. We did observe growth
292 inhibition due to ionic stress at far higher salt concentrations (500 mM NaCl). Notably,
293 cells were not sensitive to an equivalent osmotic stress (1M sorbitol), indicating the
294 sensitivity is to ionic stress, not osmotic stress.

295 As Δ*cwlO* mutants in the WT background were Mg^{2+} insensitive, we sought to
296 identify which hydrolases caused cells to be sensitive to Mg^{2+} when they were removed.
297 To find these hydrolases, we returned to intermediate strains used to construct the Δ40

298 strain, which are missing subsets of hydrolases. We transformed a *cwlO* knockout into
299 these intermediate strains, then screened these crosses for the same small colony
300 phenotype and the Mg^{2+} sensitivity seen in the Δ40 Δ*cwlO* strain. This identified two
301 genes: *yabE* and *ydjM*. Notably, during construction of the Δ40 strain, we had noticed
302 that *yocH* seemed significant – at several intermediate verification steps, a WT copy of
303 *yocH* had reintegrated itself during transformation with genomic DNA from single KO
304 strains – we therefore used PCR product for all transformations after this. Furthermore,
305 a Δ*ydjM* Δ*yocH* Δ*cwlO* mutant was previously demonstrated to be sick, with short and
306 sometimes anucleate cells (10). Because *yabE*, *ydjM*, and *yocH* have similar hydrolase
307 domains, and because *yocH* and *ydjM* had been identified previously to be involved in a
308 synthetic sick interaction with *cwlO,* we additionally tested whether the removal of *yocH*
309 contributed to the Δ40 Δ*cwlO* Mg^{2+} sensitivity phenotype, and found that it did.
310 In total, we identified three genes, *yabE*, *ydjM*, and *yocH*, whose absence in a
311 Δ*cwlO* background caused the Mg^{2+} sensitivity: A Δ*yabE* Δ*ydjM* Δ*yocH* Δ*cwlO* strain
312 showed a similar stress profile to Δ40 Δ*cwlO*, including sensitivity to $MgCl_2$ and $CaCl_2$
313 (Figure 6A). *yabE*, *ydjM*, and *yocH* are 3 uncharacterized RlpA-like superfamily domain-
314 containing proteins expressed during exponential growth. Like *lytE* and *cwlO, yocH* and
315 *ydjM* are in the *walR* regulon, while *yabE* is regulated by *sigA* (Table 1). All are likely
316 lytic transglycosylases: *yocH* has been shown to have lytic activity and has homology to
317 the *E. coli* lytic transglycosylase *mltA* (35), and all three share a similar catalytic domain.
318 Because *yabE*, *ydjM*, and *yocH* all contain a RlpA-like protein domain, we refer to these
319 genes collectively as RLPAs, and to the triple deletion of all three genes as ΔRLPAs.

320 **LytE is inhibited by Mg^{2+} *in vitro* and *in vivo*, and RLPAs suppress Mg^{2+} lethality *in*
321 *vivo***

322 Finally, we sought to identify the source of Mg^{2+} growth inhibition in the ΔRLPAs
323 Δ*cwlO* background. Because LytE is essential in the absence of CwlO, we hypothesized
324 that the sensitivity of the Δ40 Δ*cwlO* strain to Mg^{2+} (and, by extension, the sensitivity of
325 the ΔRLPAs Δ*cwlO* strain to Mg^{2+}) could be explained by Mg^{2+} inhibition of LytE. To
326 investigate this, we first characterized the response of Δ*cwlO* cells to the removal of
327 LytE. We constructed an otherwise wildtype strain with *cwlO* knocked out and *lytE*
328 under inducible control and monitored its growth by time-lapse phase-contrast
329 microscopy. When *lytE* was induced, cell growth was normal (Movie S1). When *lytE*
330 induction was removed, cell growth initially slowed, followed by a period of 'stuttery'
331 growth, where elongating cells intermittently shrank while showing accompanying
332 fluctuations in their phase contrast signal (Movie S2). Ultimately, cells lysed about 1-2
333 doubling times after the removal of *lytE* induction, as previously observed (10, 12). Next,
334 we performed the same imaging in the ΔRLPAs Δ*cwlO* strain after the addition of 10
335 mM $MgCl_2$ and observed the same 'stuttery' phenotype, suggesting that LytE function
336 might be inhibited by Mg^{2+} (Movie S4). Without the addition of Mg^{2+}, cell growth of the
337 ΔRLPAs Δ*cwlO* strain was normal (Movie S3). In WT cells or Δ*cwlO* cells, the presence
338 of Mg^{2+} has no effect on cell viability or growth – growth is only inhibited in the absence
339 of the RLPAs. Thus, the RLPAs appear to allow LytE to maintain its activity in the
340 presence of Mg^{2+}. This ΔRPLAs ΔcwlO strain additionally had a similar environmental
341 stress response profile as the Δ40 ΔcwlO strain (Figure 7A).

342 To test whether LytE activity is directly inhibited by Mg^{2+}, we overexpressed and
343 purified both full-length LytE and a truncated LytE protein with only its catalytic domain.
344 *In vitro* activity assays with and without the addition of Mg^{2+} showed that indeed LytE
345 activity is inhibited by Mg^{2+} (Figure 7B). Additionally, we reasoned that if the Mg^{2+}-
346 sensitivity phenotype was due to direct inhibition of LytE by Mg^{2+}, increasing the levels
347 of LytE should protect cells from death by increasing the total amount of LytE activity.
348 Indeed, overexpression of LytE allowed the ΔRLPAs strain to survive in the presence of
349 higher levels of Mg^{2+}, although 100 mM $MgCl_2$ still inhibited growth (Figure 7C).
350 Thus, we conclude that LytE activity is inhibited by Mg^{2+} both *in vivo* and *in vitro*.
351 Furthermore, our data indicates that the RPLAs allow LytE to maintain normal function
352 in the presence of Mg^{2+}, though the specific mechanism is unclear. Whether the RLPAs
353 act directly or indirectly on LytE remains to be determined, but we anticipate that the
354 RLPAs interact with and activate LytE similar to what has been observed for the
355 *Mycobacterium smegatis* hydrolases RipA and RpfB: RipA's C-terminus (containing a
356 NLPC/P60 domain like LytE) interacts with RpfB's RlpA-like LTG domain (36), and RipA
357 and RpfB have synergistic activity *in vitro* (37). By analogy, LytE's catalytic NLPC/P60
358 domain may interact with the RlpA-like domains in YabE, YdjM, and YocH, leading to
359 increased LytE activity, allowing LytE to continue to function in the presence of Mg^{2+}.
360 The ΔRLPAs Δ*cwlO* strain also has increased sensitivity to ionic stress and low
361 temperatures, suggesting RLPAs might stimulate LytE activity under those conditions as
362 well.

363 **DISCUSSION**

364 Bacterial cell growth requires the action of PG hydrolases, but previous *in vivo*
365 hydrolase studies have been impeded by their diversity and redundancy. We
366 constructed and validated a *B. subtilis* strain lacking all hydrolases potentially involved
367 in cell growth besides LytE and CwlO. These deletions constitute 40 genes in total,
368 representing 10% of secreted proteins and 1% of all genes. The resulting Δ40 strain
369 enables the investigation of given hydrolases and the cellular contexts in which they
370 function, and in this work, allowed several new discoveries regarding their sufficiency,
371 regulation, and genetic interplay.
372 First, we found that the Δ40 strain is viable. This demonstrates that LytE and
373 CwlO alone can function to expand the cell wall to allow cell growth. Furthermore, as
374 single knockouts of LytE and CwlO in the Δ40 strain are viable and allow growth (albeit
375 at a somewhat reduced rates with some shape defects), this demonstrates *B. subtilis*
376 requires only one of these two hydrolases to grow.
377 Our minimal hydrolase strain allowed us to show that RlpA-like lytic
378 transglycosylases enhance LytE activity *in vivo* and that this enhancement can be
379 important for growth under conditions where LytE activity is inhibited, including the
380 presence of divalent cations, ionic stress, and cold. Although the mechanism for LytE
381 enhancement is unclear, we hypothesize that RlpAs stimulate LytE activity via a direct
382 interaction, as has been observed for similar proteins in *M. smegmatis* (37). Synthetic
383 lethal or synthetic sick interactions are straightforward to identify and characterize in the
384 Δ40 strain, giving a useful tool to interrogate genetic relationships between different
385 hydrolases or between hydrolases and other genes of interest – such as those involved
386 in cell wall synthesis.

387 Surprisingly, the growth rate of the Δ40 strain is only slightly impaired under
388 standard lab conditions. What, then, is the function of these 40 hydrolases, and why
389 does *B. subtilis* encode so many of them? This multitude of hydrolases likely arises from
390 the fact that hydrolases are involved in other processes aside from cell growth such as
391 sporulation (4) and cell motility (38). Additionally, some hydrolases might be only be
392 needed under nutrient conditions not tested here, such as during phosphate limitation
393 where teichoic acids are not produced, where cells may require hydrolases that are not
394 regulated by teichoic acids (39–41). Finally, these other hydrolases may be important
395 during non-exponential growth states such as during stationary phase, where the
396 recycling of cell wall turnover products, lacking in the Δ40 strain, reduces cell lysis (42).
397 Thus, a broader screen of the sensitivity of the Δ40 strain in different nutrient and
398 environmental conditions will allow the determination of which hydrolases are useful for
399 which conditions.
400 In summary, the Δ40 minimal hydrolase strain provides a powerful experimental
401 background to investigate the function, regulation, and interplay of hydrolases,
402 improving our understanding of precisely how these enzymes conduct their cellular
403 tasks. In the future, individual hydrolases can be reintroduced into the Δ40 strain to
404 investigate their specific activities in the absence of confounding contributions from the
405 other 39 genes. Using the Δ40 strain, PG profiling can determine the biochemical
406 activity of hydrolases. Uncovering synthetic genetic interactions between hydrolases
407 and other genes of interest – now easy to do for all 40 hydrolases at once – will allow us
408 to flesh out our understanding of bacterial cell growth. Understanding the function of cell

409 wall hydrolases is essential for a complete understanding of how bacteria grow, and the
410 Δ40 strain will allow rapid progress to this end.

411 **ACKNOWLEDGEMENTS**

412 We would like to thank Carl Wivagg, Alex Bisson, Matthew Holmes, Ferran
413 Garcia-Pichel, and Susanne Neuer for helpful advice and discussions, and Georgia
414 Squyres for both helpful advice, discussions, and reading of the manuscript. We thank
415 David Rudner and Yannik Brunet for plasmids. This work was funded by National
416 Institutes of Health Grants DP2AI117923-01 to ECG, as well as support from the
417 Volkswagen Foundation. This work was supported by the NSF-Simons Center for
418 Mathematical and Statistical Analysis of Biology at Harvard (1764269) and the Harvard
419 Quantitative Biology Initiative. Some work was performed at the Center for Nanoscale
420 Systems at Harvard University, supported by NSF ECS-0335765. HPLC-MS work was
421 performed by the Harvard Center for Mass Spectrometry Core Facility, and sequencing
422 was performed by the Bauer Core Facility at Harvard University. We also acknowledge
423 the support of the Wellcome Trust (212197/Z/19/Z).

424

425 **METHODS**

426 **Strains, media, and growth conditions**

427 Glycerol stocks stored at -80˚C were struck onto LB agar plates. For strain
428 bSW61 (*lytE::pSpac-lytE,* Δ*cwlO*), these plates were additionally top spread with 1 mM
429 IPTG. After incubation overnight at 37˚C, colonies were inoculated into 1 mL media (the
430 specific media used depended on the experiment, see figure legends for details) and
431 grown on a roller at 37˚C until they reached mid-exponential-phase growth (OD_{600} ~0.2).
432 Cells were diluted 1:10 in prewarmed media and again grown until mid-exponential
433 phase; this process was repeated until the start of the experiment. Alternately, a 1:10
434 dilution series of cells were grown overnight in media on a roller at 25˚C. The next day,
435 the culture whose OD_{600} was nearest to 0.2 was diluted 1:10 and grown in media at
436 37˚C as above. $S7_{50}$AA indicates $S7_{50}$ media with added amino acids as in (43). CH
437 indicates casein hydrolysate media, as in (44). LB indicates Luria Broth (Lennox) media
438 for liquid media experiments and Luria Broth (Miller) for solid media (plates).

439 **Strain construction**

440 The wild type strain for this work was *B. subtilis* PY79. Strains used in this study
441 are listed in Table S4. Constructs were created using Gibson assembly of PCR
442 products. Linear Gibson assembly products were transformed into competent *B. subtilis*.
443 Transformants were selected on LB plates containing the appropriate antibiotic. The
444 resulting strains were verified by PCR. Constructs used in this study, as well as any
445 plasmids used to create each construct, are listed in Table S4. Primers, along with
446 strain construction details, are listed in Table S5. Resistance cassettes and promoters

447 were amplified from purified plasmids (listed in Table S4), all other fragments were
448 amplified from WT gDNA.
449 To combine knockouts, the parent strain was transformed with PCR product
450 containing the locus (homology arms + resistance cassette) or gDNA as indicated. All
451 resistance cassettes used have loxP sites flanking the cassette, allowing Cre-based
452 loop out using plasmid pDR244 (a gift from David Rudner) of the cassette to yield a
453 markerless knockout. Removal of the plasmid was accomplished by shifting streaks to
454 42˚C where it cannot be replicated due to a temperature-sensitive origin. Successful
455 loop outs were confirmed via loss of antibiotic resistance.
456 **PHMMER search**
457 We used pfamscan version 1.6 to search the *B. subtilis* 168 and PY79 proteomes
458 for all pfam domains using default parameters: e-value: 0.01, significance E-values [hit]:
459 0.03, significance bit scores [sequence]: 25, significance bit scores [hit]: 22. We then
460 filtered the list for domains of interest using the list of domains in Table S2, and
461 identified putative membrane-bound/cytoplasmic proteins using UniProt (45).
462 **PG purification, HPLC conditions, and MS data analysis**
463 PG purification was conducted as in (46), with an HF treatment step instead of
464 HCl to remove teichoic acids and the addition of a protein digestion step. Cells were
465 grown in a baffled flask to an OD_{600} of ~0.5 in 50 mL of CH media. Cells were mixed
466 50/50 with 50 mL of boiling 10% SDS and boiled for 15 min in a water bath, then
467 pelleted at 5000x g and washed 5x with ddH2O. Cells were then resuspended in 2 mL
468 DNAse/RNase buffer (10 mM Tris pH 7.5, 2.5 mM $MgCl_2$, 0.5 mM $CaCl_2$) with 20 µL
469 DNAse I and 20 µL RNAse A, then incubated overnight at 37˚C and washed 3x with

470 ddH2O to remove nucleic acids. Next, cells were resuspended in 2 mL Proteinase K
471 buffer (10 mM Tris pH 7.5, 1 mM $CaCl_2$) with 20 µL Proteinase K, incubated overnight at
472 45^0C, and washed 3x with ddH2O to remove proteins. Next, cell walls were treated with
473 48% (v/v) hydrofluoric acid on ice for 24H, then washed twice with 100 mM Tris pH 8
474 and 4 times with ddH2O. Then, the PG was resuspended in 12.5 mM $NaHPO_4$ pH 5.5
475 with 5000 units of mutanolysin and digested overnight (16h) at 37˚C on a roller to yield
476 soluble muropeptides. Undigested material was pelleted by spinning at 16000x g for 5
477 mins and the supernatant was transferred to a new tube. Soluble muropeptides were
478 reduced with sodium borohydride (1 mg/mL) for 30 mins and the reaction was stopped
479 by adding 10 µL 30% phosphoric acid. The pH was adjusted to 4-6 using NaOH, and
480 the reduced soluble muropeptides were characterized by high-resolution LC-MS
481 operating in both positive and negative mode. Soluble reduced muropeptides were
482 separated on a Waters column with the following method: column temperature 52˚C,
483 flow rate 0.5 mL/min, linear gradient of solvent A (0.1% (w/v) formate) to 10% solvent B
484 (acetonitrile + 0.1% (w/v) formate) over 80 min.
485 Feature detection was performed on the raw MS data using Dinosaur (47).
486 Feature detection was done separately on both the positive and negative mode scans
487 with default parameters. Feature data were analyzed using a custom MATLAB program,
488 available at https://bitbucket.org/garnerlab/wilson_40_2020/. We first filtered feature
489 data for charge < 3. Next, we filtered for the top 10 features present during each scan.
490 For each of these features, theoretical m/z values were compared with observed m/z
491 with a cutoff of 10 ppm. We required that a compound be present on both the positive
492 and negative scans, and consolidated features matching the same compound within a

493 retention time within 1 min. Finally, we filtered out compounds corresponding to in-
494 source decay (loss of glucosamine without a change in retention time), and compounds
495 present at less than 0.1% of all muropeptides. Retention times shown in Table S3 were
496 analyzed manually.

497 **Growth rates**

498 Cells were grown to an OD_{600} of ~0.3-0.5 on a roller drum at 37˚C and diluted to
499 an OD_{600} of ~0.05 in baffled flasks in a water bath shaker at 37˚C. Samples were
500 withdrawn at 5 min intervals and OD_{600} was measured in a plastic cuvette using a
501 Biowave Cell Density Meter CO8000. T vs. OD_{600} curves were fit to a single exponential
502 ($OD_{600} = Ae^{BT}$) to extract a growth rate (B).

503 **Autolysis rates**

504 Cells were grown to an OD_{600} of ~0.3-0.5 on a roller drum at 37˚C and diluted to
505 an OD_{600} of ~0.025 into prewarmed CH in baffled flasks at 37˚C. Once cells reached an
506 OD_{600} of 0.5, sodium azide (75 mM final) or ampicillin (100 µg/mL final) was added to
507 part of culture and transferred to a prewarmed 96 well plate. OD_{600} was measured every
508 2 minutes for 24H at 37˚C using a BioTek Epoch 2 Microplate Spectrophotometer. The
509 plate was shaken at maximum RPM in between measurements.

510 **Sporulation efficiency**

511 Sporulation was induced by resuspension according to (44). Cells were grown to
512 an OD_{600} of ~0.3-0.5 in CH media, pelleted, and resuspended in resuspension medium.
513 Sporulation efficiency was assessed by measuring the number of heat-resistant CFUs
514 per mL of culture after 36H. The cultures were heated to 80˚C for 20 mins, then plated.
515 CFU counts were then done after 24H of incubation at 37˚C.

516 **Turnover rates**

517 Turnover rates were measured as in (43) with some modifications; the method is
518 summarized below. Cells were grown in $S7_{50}AA$ to an OD_{600} of ~0.3-0.5 on a roller drum
519 at 37˚C and diluted to an OD_{600} of ~0.05 in 3 mL of prewarmed $S7_{50}AA$ containing 1 uCi
520 of ^{3}H-N-acytylglucosamine [6-^{3}H] (specific activity: 20 Ci/mmol, American Radiolabeled
521 Chemicals, Inc., St. Louis, MI, USA) in 25mm wide test tubes in a water bath shaker at
522 37˚C. Cells were labeled for 3 generations (until OD_{600} ~0.4), then filtered, washed twice
523 with prewarmed $S7_{50}AA$, and resuspended in 25 mL of prewarmed $S7_{50}AA$. Samples
524 were withdrawn at 5 min intervals and OD_{600} was measured in a plastic cuvette using a
525 Biowave Cell Density Meter CO8000. Samples were mixed 50:50 with ice cold 10%
526 (v/v) TCA + 20 mM unlabeled GlcNAc, incubated on ice for 10 mins, then filtered and
527 washed. Filters were dried, resuspended in Ultima Gold LSC cocktail (PerkinElmer,
528 Waltham, MA, USA) and radioactivity was measured using a scintillation counter (Tri-
529 Carb 2100 TR, PerkinElmer). Decays/min vs. OD_{600} plots were fit to a single exponential
530 (DPM = Ae^{BT}) to extract a turnover rate (B).

531 **Cell dimensions**

532 Cells were grown to an OD_{600} of ~0.3-0.5 in a water bath shaker at 37˚C. 1 mL of
533 culture was stained with FM 5-95 and concentrated to 100 µL by centrifugation at 2000x
534 g and resuspension. 5 µL of concentrated cells were spotted under 2% (w/v) agarose
535 pads in CH containing 0.5 ug/mL FM 5-95. Images were collected on a Nikon Ti-E
536 microscope using a Nikon CFI Plan Apo DM Lambda 100X Oil objective, 1.45 NA,
537 phase ring Ph3 using an ORCA-Flash4.0 V2 sCMOS camera. Analysis was performed
538 using Morphometrics v1.1 (48). Zero length or width cells were discarded, as well as

539 any cells with width greater than length. Outliers were removed using Graphpad Prism
540 ROUT with default parameters (1%).

541 **Chain length**

542 Cells were grown to an OD_{600} of ~0.3-0.5 on a roller drum at 37˚C and diluted to
543 an OD_{600} of ~0.025 into prewarmed CH in baffled flasks at 37˚C. Once cells reached an
544 OD_{600} of 0.5, 1-5 µl of culture was spotted under a prewarmed 2.5% (w/v) agarose pad
545 in CH. A 10x10 image tile series was collected (~1.5 mm square). A custom MATLAB
546 program was used to register and stitch the images together, and then chain length was
547 measured manually with the assistance of a custom MATLAB program.

548 **Electron microscopy and cell wall thickness measurements**

549 Electron microscopy was performed as in (49). Briefly, exponentially growing
550 cells were fixed in 100 mM MOPS buffer pH 7 containing 2% (w/v) paraformaldayde,
551 2.5% (w/v) gluteraldehyde, and 1% (v/v) dimethyl sulfoxide overnight at 4°C, washed,
552 stained with 2% (w/v) osmium tetroxide in 100 mM MOPS for 1 hr, washed, and stained
553 overnight with 2% (w/v) uranyl acetate. The cells were then dehydrated and embedded
554 in Embed 812 resin.

555 Serial ultrathin sections (80 nm) were cut with a Diatome diamond knife (EMS,
556 PA) on a Leica Ultracut UCT (Leica Microsystems, Germany) and collected on 200-
557 mesh thin-bar formvar carbon grids. Sections were imaged on a Hitatchi HT7800
558 transmission electron microscope.

559 Images collected were segmented (inner cell wall, outer cell wall) using DeepCell
560 (50), and cell wall thickness was measured using a custom Matlab program available at
561 https://bitbucket.org/garnerlab/wilson_40_2020/. Briefly, the distance between the inner

562 and outer cell wall was measured every 10 nm along a user-defined line, and the mean
563 of that measurement was taken to be the cell's cell wall thickness.

564 **AFM imaging and cell wall thickness measurement**

565 *B. subtilis* cells at mid-exponential phase were boiled rapidly to kill bacterial cells
566 & inactivate any potential hydrolase activity. Cells were broken by French Press and
567 FastPrep, then suspended in 5% (w/v) SDS and boiled for 25 min, and sacculi collected
568 by centrifugation at 20,000 g for 3 mins. The resulting pellets were washed with distilled
569 water to remove all traces of SDS, then re-suspended in Tris-HCl (50 mM, pH7)
570 containing 2 mg/ml pronase and incubated at 60°C for 90 mins. The resulting sacculi
571 were then re-suspended in LC-MS Chromasolv water for storage at -20°C.

572 Freshly cleaved mica discs were incubated with Cell-Tak™, (285 ml 100 mM
573 $NaHCO_3$ (pH 8) then 10 µl of Cell-Tak (Corning, 5% (w/v) in acetic acid) and 5 µl of 1 M
574 NaOH, covered and left for 20 minutes then washed five times with HPLC grade water)
575 to ensure attachment of sacculi on the glass surface. Sacculi were diluted in HPLC-
576 grade water to appropriate concentration and dried onto mica using N_2. These were
577 further washed and dried with N_2 again to remove any unattached sample.

578 All AFM data was taken on a JPK Nanowizard III in QI (quantitative imaging)
579 mode. Samples were imaged in HPLC Grade water using a FastScanD cantilever
580 (Bruker, Santa Barbara), nominal spring constant 0.25 N/m with a 256 x 256-pixel scan
581 region, driven at ~167 Hz with a typical Z length of ~ 300 nm using peak interaction
582 forces of 2-3 nN. Images were flattened to median of differences and first order planefit
583 using Gwyddion.

584 **Spot dilution assay**

585 Cells were grown to an OD_{600} of 0.5 and diluted 1:10 into 100 µL of LB media in a
586 96 well plate. A 1:10 serial dilution series was made, and 3 µL of each dilution was
587 spotted onto the plate using a multichannel pipettor. The plates were allowed to dry and
588 incubated in at 37˚C or 42˚C as indicated for 18h. Plates incubated at 25˚C or 18˚C
589 were left for additional time (24h and 48h, respectively). Plates were photographed
590 using a Canon SC1011 scanner with the lid open.
591 For the colony morphology assay in Figure 1, this protocol was followed except
592 that a colony of cells of each strain were simply resuspended in 100 µL of media using a
593 toothpick (omitting the broth culture step).
594 **LytE purification**
595 His-SUMO-tagged full length LytE missing the signal peptide (26-355) and His-
596 SUMO-tagged truncated LytE missing its 3x LysM domains (185-255) were
597 overexpressed and purified under denaturing conditions from E. coli BL21. 3L of LB
598 Amp culture was grown to an OD_{600} of 0.7 and overexpression was induced with 1 mM
599 IPTG. Cultures were induced for 6H, then harvested by centrifugation. Pellets were
600 frozen at -80˚C for storage. For purification, pellets were thawed and resuspended in
601 lysis buffer (100 mM sodium phosphate, 10 mM Tris, 10 mM imidazole, 1% (v/v) Trition,
602 8M Urea, pH 8). Cells were lysed by sonication, and cell debris was removed by
603 centrifugation. A His column was equilibrated in lysis buffer (3 mL bed volume). Clarified
604 lysate was passed through the His column. The bound protein was washed once with
605 50 mM HEPES, 150 mM NaCl, 20 mM imidazole, 1% (v/v) Triton, 8M Urea, pH 8.
606 Proteins were renatured on the column in 50 mM HEPES, pH 8 with 1% (v/v) Triton and
607 20 mM imidazole with a steady reduction of urea concentration (8M, 6M, 4M, 2M, 1M,

608 0M) and increasing NaCl concentration (150 mM, 237.5 mM, 325 mM, 412.5 mM,
609 456.25 mM, 500 mM). Refolded proteins were eluted from the column by increasing the
610 imidazole concentration to 250 mM. DTT was added to 1 mM to all fractions. Fractions
611 containing the target protein were pooled and dialyzed overnight at 4˚C in cleavage
612 buffer (50 mM HEPES pH 8, 500 mM NaCl, 2 mM DTT) with the addition of purified
613 Ulp1 to cleave the 6His-SUMO tag. Buffer was exchanged once and further dialyzed for
614 several hours. A new column was equilibrated in cleavage buffer without DTT and the
615 pooled, cleaved protein was run through the column to remove the 6His-SUMO tag.
616 Fractions contained cleaved protein were pooled and concentrated to a volume of 2 mL,
617 then stored in dialysis in cleavage buffer. Activity tests were performed using purified
618 PG in cleavage buffer plus 0.5% (w/v) Pluronic F-108 and PG from Sigma to an OD_{600}
619 of 0.25 at 37˚C. OD_{600} was measured every 2 minutes for 24H using a BioTek Epoch 2
620 Microplate Spectrophotometer. The plate was shaken at maximum RPM in between
621 measurements.

622 **Data availability**

623 All custom software used in this work is available at
624 https://bitbucket.org/garnerlab/wilson_40_2020/. Raw HPLC-MS data for PG profiling
625 experiments available from ftp://massive.ucsd.edu/MSV000086886
626 (doi:10.25345/C5R21D). Raw and error corrected sequencing reads for whole genome
627 sequencing available at https://www.ncbi.nlm.nih.gov/Traces/study/?acc=PRJNA702153
628 (BioProject PRJNA702153).

629

630

Table 1: List of cell wall hydrolases in *Bacillus subtilis* identified using PHMMER. Cell wall hydrolases were identified via a PHMMR (13) search with default parameters of the *B. subtilis* subsp. 168 and *B. subtilis* subsp. PY79 proteome for PFAM domains associated with known cell wall hydrolases (Table S2). For each hydrolase, we report its name (and any aliases), whether it is knocked out in the Δ40 strain (KO) or present in PY79 (Y/N), its UniProt accession number, its locus tag, any reported regulons it is a member of (^ indicates source Faria et al. 2016, * indicates source SubtiWiki (97)), the PHMMR search significance e-value, and any relevant references showing its biochemical activity. Abbreviations: DLEP, D,L-endopeptidase; LDEP, L,D-endopeptidase; DDEP, D,D-endopeptidase; LTG, lytic transglycosylase; SU, specificity untested (only cell wall degradative activity shown). **CwlP and CwlT are two-domain cell wall hydrolases and so appear twice on this table. Only the activity for the specific PFAM domain is listed in the Activity column.

645 **Figure 1: Construction of the Δ40 strain via sequential knockout and loopout.**
646 Colony morphology of each cloning intermediate for the Δ40 strain. WT cells were
647 transformed with a series of resistance-cassette-marked knockouts (starting with
648 Δ*cwlQ*). Periodically, antibiotic resistance cassettes were removed via Cre-loxP
649 mediated loopout (indicated by LO). Arrows indicate sequential integrations (e.g., the
650 strain indicated by Δ*yocH* contains Δ*yocH* and Δ*cwlQ*). Dense cell suspensions were
651 spotted and incubated overnight to visualize colony morphology.
652
653 **Figure 2: The Δ40 strain has a reduced cell wall hydrolytic complement**
654 **A: HPLC analysis of isolated muropeptides in WT and Δ40 strains.** Purified cell
655 walls were digested to yield soluble muropeptides which were separated and
656 characterized via HPLC-MS. The total ion current (TIC) elution profile is shown. Strains
657 used: PY79, WT; bSW431, Δ40; bSW537, Δ40 Δ*mltG*.
658 **B: Identification of cell wall hydrolase products in WT and Δ40 cells by**
659 **peptidoglycan profiling**. High-resolution mass spectrometry was used to identify
660 separated muropeptides. Muropeptides missing a GlcNAc were classified as
661 glucosaminidase products. Anhydromuropeptides were classified as LTG products.
662 Crosslinked muropeptides lacking MurNAc-GlcNAc and MurNAc-GlcNAc itself was
663 classified as amidase products. Crosslinked muropeptides lacking MurNAc-GlcNAc-L-
664 Ala-iso-D-Glu, and MurNAc-GlcNAc-L-Ala-iso-D-Glu itself, was classified as D,L-
665 endopeptidase products. For additional details about muropeptide classification, see
666 Supplemental Table 2. Crosslinking index was calculated as in (98). For each set of
667 hydrolase products, the sum of the MS intensity for those products was divided by the

668 total MS intensity for all detected muropeptides (% of total). D,L-endopeptidase
669 products are still present as expected, because the strain retains the D,L-
670 endopeptidases LytE and CwlO. Amidase products are strongly reduced.
671 Glucosaminidase products are reduced in abundance by roughly twofold. Lytic
672 transglycosylase products are still present in the Δ40 strain but are strongly reduced if
673 *mltG* is additionally knocked out. Strains used: PY79, WT; bSW431, Δ40; bSW537, Δ40
674 Δ*mltG*.
675
676 **Figure 3: The Δ40 strain grows at a similar rate as WT cells, does not sporulate,**
677 **and has a much slower autolysis rate in response to both sodium azide and**
678 **ampicillin.**
679 **A (left): The Δ40 strain has a slower growth rate vs WT in LB media.** Cultures were
680 grown in LB media at 37˚C to an OD_{600} of ~0.3-0.5, diluted to an OD_{600} of 0.05, and
681 samples were collected every 6 minutes for 1 hrs (~3 doublings). OD_{600} vs time plots
682 were fit to a single exponential to obtain the growth rate. Each point represents the
683 doubling time from a single experiment, and solid lines show mean and standard
684 deviation. The dotted line shows the mean WT growth rate, for comparison. Δ40 has a
685 slower growth rate to WT. *lytE* and *cwlO* knockouts grow much more slowly in the Δ40
686 background than in a WT background. Strains used: PY79, WT; bSW23, Δ*cwlO*;
687 bSW295, Δ*lytE*; bSW431, Δ40; bSW433, Δ40 Δ*cwlO*; bSW435, Δ40 Δ*lytE*.
688 **A (middle): The Δ40 strain has a similar growth rate to WT in CH media.** Cultures
689 were grown in CH media at 37˚C. Samples were collected and data was analyzed as in
690 (A). While Δ40 has a similar growth rate to WT, *lytE* and *cwlO* knockouts grow more

691 slowly in this background than in a WT background. Strains used: PY79, WT; bSW23,
692 Δ*cwlO*; bSW295, Δ*lytE*; bSW431, Δ40; bSW433, Δ40 Δ*cwlO*; bSW435, Δ40 Δ*lytE*.
693 **A (right): The Δ40 strain has a similar growth rate to WT in minimal media.**
694 Cultures were grown in $S7_{50}AA$ media at 37˚C. Samples were collected and data was
695 analyzed as in (A). Strains used: PY79, WT; bSW431, Δ40.
696 **B: The Δ40 strain is unable to sporulate.** Sporulation was induced by resuspension
697 and sporulation efficiency was determined as in (24). The WT strain produced ~10^8
698 spores/mL while the Δ40 strain produced ~100 spores/mL, all of which lacked the
699 distinctive Δ40 colony morphology and likely represent contamination. Strains used:
700 PY79, WT; bSW431, Δ40.
701 **C: The Δ40 strain shows slower autolysis in response to sodium azide (left) and**
702 **ampicillin (right).** Cultures were grown in CH media at 37˚C to an OD_{600} of 0.5 (azide
703 treatment) or 0.15 (ampicillin treatement) in baffled flasks with vigorous shaking, then
704 diluted to an OD_{600} of 0.025 in a 150 µL of prewarmed CH in a 96-well plate. Sodium
705 azide (75 mM) or ampicillin (100 µg/mL) was added and OD_{600} readings were taken
706 using a plate reader every 2 minutes for 24H. The plate was shaken vigorously in
707 between measurements. The Δ40 strain takes around 10 times as long to reach half the
708 intial OD_{600} as the WT strain, and the Δ40 ΔlytE strain in particular has a strongly
709 reduced rate of autolysis. Strains used: PY79, WT; bSW23, Δ*cwlO*; bSW295, Δ*lytE*;
710 bSW431, Δ40; bSW433, Δ40 Δ*cwlO*; bSW435, Δ40 Δ*lytE*.
711
712 **Figure 4: The Δ40 strain has mild shape defects but a significant chaining**
713 **phenotype.**

714 **A: Representative phase contrast images of hydrolase mutant strains.** Δ40 cells
715 primarily form long chains, Δ40 Δ*cwlO* cells have variable widths, and Δ40 Δ*lytE* cells
716 sometimes have phase-light, lysed cells still attached to their poles (see Figure S2 for
717 TEM images). Both Δ40 Δ*cwlO* and Δ40 Δ*lytE* have a population of phase-light, lysed
718 cells. Scale bar is 10 μm.
719 **B: Cell lengths (left) and widths (right) in hydrolase mutants.** Cells were labeled
720 with membrane stain and imaged by epifluorescence microscopy. Cell dimensions were
721 measured from these images using Morphometrics. Solid lines in violins show medians.
722 Dashed line outside violins shows WT median for comparison. Shaded region outside
723 violins shows WT quartiles. Strains used: PY79, WT; bSW23, Δ*cwlO*; bSW295, Δ*lytE*;
724 bSW431, Δ40; bSW433, Δ40 Δ*cwlO*; bSW435, Δ40 Δ*lytE*.
725 **C: Chain lengths in hydrolase mutants (left, zoomed view of right).** Chain length
726 was measured manually from tiled and stitched phase contrast images. The Δ40 strain's
727 median chain length is around 30 times longer than the WT median chain length.
728 Strains used: PY79, WT; bSW23, Δ*cwlO*; bSW295, Δ*lytE*; bSW431, Δ40; bSW433, Δ40
729 Δ*cwlO*; bSW435, Δ40 Δ*lytE*.
730
731 **Figure 5: The Δ40 strain does not detectably turn over cell wall.**
732 **A: Cell wall turnover rate is negligible in the Δ40 strain.** *Left*: Pulse-chase radiolabel
733 measurements were used to determine the cell wall turnover rate. Cells were labeled
734 with H^3-GlcNAc, which incorporates into the cell wall. The ^{3}H-GlcNAc was then washed
735 out and radioactivity was subsequently measured for 3 generations. A decrease in
736 radioactivity indicates that material is being removed from the cell wall, e.g. that cell wall

737 is turning over. Each experiment was replicated at least 3 times. Dotted lines show
738 single exponential fit to mean data. *Right*: Single exponential fits to each experiment at
739 left. Each point represents the time constant (-k) obtained from a fit to a single
740 experiment. Error bars show SD. The Δ40 turnover rate is not significantly different from
741 zero (one sample t test, p=0.4837). Mean initial radioactivity was 167766 DPM/OD_{600} for
742 the WT strain and 174334 DPM/OD_{600} for the Δ40 strain. Strains used: PY79, WT;
743 bSW431, Δ40.
744 **B: Cell wall thickness in the Δ40 strain.** Cell wall thickness was measured via
745 transmission electron microscopy and atomic force microscopy as described in
746 Methods. Briefly, for TEM imaging, exponentially growing cells were fixed, osmicated,
747 stained with uranyl acetate, embedded in Embed 812, sectioned, and imaged without
748 additional staining. For AFM imaging, exponentially growing cells were boiled, broken,
749 protease treated, and then adhered to mica for imaging. Each point is the mean cell wall
750 thickness measured for a single cell. WT AFM measurements are reproduced from (99),
751 Δ40 AFM measurements were performed as part of this study. Error bars show SD.
752 Strains used: PY79, WT (for TEM measurements); 168, WT (for AFM measurements);
753 bSW431, Δ40.
754 **C: Representative TEM images of cell wall thickness.** Representative TEM images
755 of cell wall thickness analyzed in B. Strains used: PY79, WT; bSW431, Δ40. Scale bar
756 is 20 nm.
757 **D: Representative AFM images of sacculi.** Representative AFM images of cell walls
758 analyzed in B. Strains used: 168, WT; bSW431, Δ40. Scale bars are 100 nm.
759

760 **Figure 6: The Δ40 strain has similar viability to WT in a range of stress conditions,**
761 **but Δ40 Δ*cwlO* is sensitive to ionic, cold, and low pH stress.** Spot dilution assays of
762 different strains under various stress conditions. Cultures of each strain were plated in a
763 1:10 dilution series onto LB plates containing various stressors and grown overnight at
764 the specified temperature, or at 37˚C if not indicated. Most conditions supported normal
765 growth, but growth of the Δ40 Δ*cwlO* strain was inhibited at 25˚C, pH 5.5, or with the
766 addition of 10 mM $MgCl_2$, 10 mM $MgSO_4$, 10 mM $CaCl_2$, or 300 mM NaCl. Strains used:
767 PY79, WT; bSW23, Δ*cwlO*; bSW295, Δ*lytE*; bSW431, Δ40; bSW433, Δ40 Δ*cwlO*;
768 bSW435, Δ40 Δ*lytE*.
769
770 **Figure 7: Three uncharacterized RlpA-like proteins stimulate LytE activity in the**
771 **presence of divalent cations.**
772 **A: The removal of three RlpA-like proteins makes Δ*cwlO* cells stress-sensitive.**
773 Spot dilution assays were performed as in Figure 4. Δ*yabE* Δ*yocH* Δ*ydjM* (ΔRLPAs)
774 Δ*cwlO* showed the same stress sensitivity profile as Δ40 Δ*cwlO*, except that 10 mM
775 $MgSO_4$ and 25˚C only partially inhibited growth. Strain used: bSW490, Δ*cwlO* Δ*yabE*
776 Δ*yocH* Δ*ydjM*.
777 **B: Mg^{2+} directly inhibits LytE activity.** LytE was expressed in E. coli and purified both
778 with and without its N-terminal LysM domains and incubated with purified cell walls in
779 150 µL of 50 mM HEPES pH 7, 2 mM DTT, 500 mM NaCl with 0.5% (w/v) Pluronic F-
780 108 in a 96-well plate. OD_{600} was measured every 2 min using a plate reader. The
781 addition of 25 mM $MgCl_2$ almost completely inhibited the activity of LytE.

782 **C: LytE overexpression rescues Mg^{2+} sensitivity in the ΔRLPAs Δ*cwlO***

783 **background.** Spot dilutions were performed as in Figure 5A, with the indicated

784 concentration of $MgCl_2$ and the addition of 1 mM IPTG to drive LytE overexpression.

785 Strains used: PY79, WT; (ΔRLPAs) Δ*cwlO*, bSW490, Δ*cwlO* Δ*yabE* Δ*yocH* Δ*ydjM*;

786 (ΔRLPAs) Δ*cwlO* lytE overexpression, bSW519, Δ*cwlO* Δ*yabE* Δ*yocH* Δ*ydjM*

787 *amyE::pHyperSpank-lytE*.

788

789

790 **REFERENCES**

791 1. Brill J, Hoffmann T, Bleisteiner M, Bremer E. 2011. Osmotically controlled
792 synthesis of the compatible solute proline is critical for cellular defense of Bacillus
793 subtilis against high osmolarity. J Bacteriol 193:5335–5346.
794 2. Vollmer W. 2012. Bacterial growth does require peptidoglycan hydrolases. Mol
795 Microbiol 86:1031–1035.
796 3. Typas A, Banzhaf M, Gross CA, Vollmer W. 2012. From the regulation of
797 peptidoglycan synthesis to bacterial growth and morphology. Nat Rev Microbiol
798 10:123–136.
799 4. Smith TJ, Blackman SA, Foster SJ. 2000. Autolysins of Bacillus subtilis: Multiple
800 enzymes with multiple functions. Microbiology 146:249–262.
801 5. Vermassen A, Leroy S, Talon R, Provot C, Popowska M, Desvaux M. 2019. Cell
802 wall hydrolases in bacteria: Insight on the diversity of cell wall amidases,
803 glycosidases and peptidases toward peptidoglycan. Front Microbiol 10.
804 6. Dik DA, Marous DR, Fisher JF, Mobashery S. 2017. Lytic transglycosylases:
805 concinnity in concision of the bacterial cell wall. Crit Rev Biochem Mol Biol
806 52:503–542.
807 7. Blackman SA, Smith TJ, Foster SJ. 1998. The role of autolysins during vegetative
808 growth of Bacillus subtilis 168. Microbiology 144:73–82.
809 8. Holtje J V. 1995. From growth to autolysis: The murein hydrolases in Escherichia
810 coli. Arch Microbiol 164:243–254.
811 9. Heidrich C, Ursinus A, Berger J, Schwarz H, Höltje JV. 2002. Effects of multiple
812 deletions of murein hydrolases on viability, septum cleavage, and sensitivity to

813 large toxic molecules in Escherichia coli. J Bacteriol 184:6093–6099.
814 10. Bisicchia P, Noone D, Lioliou E, Howell A, Quigley S, Jensen T, Jarmer H, Devine
815 KM. 2007. The essential YycFG two-component system controls cell wall
816 metabolism in Bacillus subtilis. Mol Microbiol 65:180–200.
817 11. Fukushima T, Afkham A, Kurosawa SI, Tanabe T, Yamamoto H, Sekiguchi J.
818 2006. A new D,L-endopeptidase gene product, YojL (renamed CwlS), plays a role
819 in cell separation with LytE and LytF in Bacillus subtilis. J Bacteriol 188:5541–
820 5550.
821 12. Meisner J, Llopis PM, Sham LT, Garner E, Bernhardt TG, Rudner DZ, Montero
822 Llopis P, Sham LT, Garner E, Bernhardt TG, Rudner DZ. 2013. FtsEX is required
823 for CwlO peptidoglycan hydrolase activity during cell wall elongation in Bacillus
824 subtilis. Mol Microbiol 89:1069–1083.
825 13. Potter SC, Luciani A, Eddy SR, Park Y, Lopez R, Finn RD. 2018. HMMER web
826 server: 2018 update. Nucleic Acids Res 46:W200–W204.
827 14. Skovgaard O, Bak M, Løbner-Olesen A, Tommerup N. 2011. Genome-wide
828 detection of chromosomal rearrangements, indels, and mutations in circular
829 chromosomes by short read sequencing. Genome Res 21:1388–1393.
830 15. Atrih A, Bacher G, Allmaier G, Williamson MP, Foster SJ. 1999. Analysis of
831 Peptidoglycan Structure from Vegetative Cells of Bacillus subtilis 168 and Role of
832 PBP 5 in Peptidoglycan Maturation. J Bacteriol 181:3956–3966.
833 16. Yunck R, Cho H, Bernhardt TG. 2016. Identification of MltG as a potential
834 terminase for peptidoglycan polymerization in bacteria. Mol Microbiol 99:700–718.
835 17. Sassine J, Pazos M, Breukink E, Vollmer W. 2021. Lytic transglycosylase MltG

836 cleaves in nascent peptidoglycan and produces short glycan strands. Cell Surf
837 7:100053.
838 18. Taguchi A, Page JE, Tsui HCT, Winkler ME, Walker S. 2021. Biochemical
839 reconstitution defines new functions for membrane-bound glycosidases in
840 assembly of the bacterial cell wall. Proc Natl Acad Sci U S A 118:1–10.
841 19. Jolliffe LK, Doyle RJ, Streips UN. 1981. The energized membrane and cellular
842 autolysis in Bacillus subtilis. Cell 25:753–763.
843 20. Margot P, Pagni M, Karamata D. 1999. Bacillus subtilis 168 gene lytF encodes a
844 7-D- muropeptidase expressed by the alternative vegetative sigma factor , cD.
845 Microbiology 145:57–65.
846 21. Ohnishi R, Ishikawa S, Sekiguchi J. 1999. Peptidoglycan hydrolase LytF plays a
847 role in cell separation with CwlF during vegetative growth of Bacillus subtilis. J
848 Bacteriol 181:3178–3184.
849 22. Ishikawa S, Hara Y, Ohnishi R, Sekiguchi J. 1998. Regulation of a new cell wall
850 hydrolase gene, cwlF, which affects cell separation in Bacillus subtilis. J Bacteriol
851 180:2549–2555.
852 23. Heffron JD, Orsburn B, Popham DL. 2009. Roles of Germination-Specific Lytic
853 Enzymes CwlJ and SleB in Bacillus anthracis. J Bacteriol 191:2237–2247.
854 24. Chastanet A, Losick R. 2007. Engulfment during sporulation in Bacillus subtilis is
855 governed by a multi-protein complex containing tandemly acting autolysins. Mol
856 Microbiol 64:139–152.
857 25. Morlot C, Uehara T, Marquis KA, Bernhardt TG, Rudner DZ. 2010. A highly
858 coordinated cell wall degradation machine governs spore morphogenesis in

859 Bacillus subtilis. Genes Dev 24:411–422.
860 26. Pooley HM. 1976. Layered distribution, according to age, within the cell wall of
861 bacillus subtilis. J Bacteriol 125:1139–1147.
862 27. Fan DP, Beckman MM. 1971. Mutant of Bacillus subtilis demonstrating the
863 requirement of lysis for growth. J Bacteriol 105:629–636.
864 28. Fan DP, Beckman MM, Cunningham WP. 1972. Ultrastructural studies on a
865 mutant of Bacillus subtilis whose growth is inhibited due to insufficient autolysin
866 production. J Bacteriol 109:1247–1257.
867 29. Graham LL, Beveridge TJ. 1990. Evaluation of freeze-substitution and
868 conventional embedding protocols for routine electron microscopic processing of
869 eubacteria. J Bacteriol 172:2141–2149.
870 30. Graham LL, Beveridge TJ. 1994. Structural differentiation of the Bacillus subtilis
871 168 cell wall. J Bacteriol 176:1413–1421.
872 31. Matias VRF, Beveridge TJ. 2005. Cryo-electron microscopy reveals native
873 polymeric cell wall structure in Bacillus subtilis 168 and the existence of a
874 periplasmic space. Mol Microbiol 56:240–251.
875 32. Kern T, Giffard M, Hediger S, Amoroso A, Giustini C, Bui NK, Joris B, Bougault C,
876 Vollmer W, Simorre JP. 2010. Dynamics characterization of fully hydrated
877 bacterial cell walls by solid-state NMR: Evidence for cooperative binding of metal
878 ions. J Am Chem Soc 132:10911–10919.
879 33. Hussain S, Wivagg CN, Szwedziak P, Wong F, Schaefer K, Izoré T, Renner LD,
880 Holmes MJ, Sun Y, Bisson-Filho AW, Walker S, Amir A, Löwe J, Garner EC.
881 2018. MreB filaments align along greatest principal membrane curvature to orient

882 cell wall synthesis. Elife 7:1–45.
883 34. Formstone A, Errington J. 2005. A magnesium-dependent mreB null mutant:
884 Implications for the role of mreB in Bacillus subtilis. Mol Microbiol 55:1646–1657.
885 35. Shah IM, Dworkin J. 2010. Induction and regulation of a secreted peptidoglycan
886 hydrolase by a membrane Ser/Thr kinase that detects muropeptides. Mol
887 Microbiol 75:1232–1243.
888 36. Hett EC, Chao MC, Rubin EJ. 2010. Interaction and modulation of two
889 antagonistic cell wall enzymes of mycobacteria. PLoS Pathog 6:1–14.
890 37. Hett EC, Chao MC, Deng LL, Rubin EJ. 2008. A mycobacterial enzyme essential
891 for cell division synergizes with resuscitation-promoting factor. PLoS Pathog 4.
892 38. Sanchez S, Dunn CM, Kearns DB. 2021. CwlQ is required for swarming motility
893 but not flagellar assembly in Bacillus subtilis. bioRxiv 2021.01.13.426625.
894 39. Calamita HG, Doyle RJ. 2002. Regulation of autolysins in teichuronic acid-
895 containing Bacillus subtilis cells. Mol Microbiol 44:601–606.
896 40. Atilano ML, Pereira PM, Yates J, Reed P, Veiga H, Pinho MG, Filipe SR. 2010.
897 Teichoic acids are temporal and spatial regulators of peptidoglycan cross-linking
898 in Staphylococcus aureus. Proc Natl Acad Sci U S A 107:18991–18996.
899 41. Yamamoto H, Miyake Y, Hisaoka M, Kurosawa SI, Sekiguchi J. 2008. The major
900 and minor wall teichoic acids prevent the sidewall localization of vegetative DL-
901 endopeptidase LytF in Bacillus subtilis. Mol Microbiol 70:297–310.
902 42. Reith J, Mayer C. 2011. Peptidoglycan turnover and recycling in Gram-Positive
903 bacteria. Appl Microbiol Biotechnol 92:1–11.
904 43. Vitkovic LA, Cheung HY, Freese E. 1984. Absence of correlation between rates of

905 cell wall turnover and autolysis shown by Bacillus subtilis mutants. J Bacteriol
906 157:318–320.
907 44. Harwood CR, Cutting SM. 1990. Molecular Biological Methods for Bacillus
908 (Modern Microbiological Methods). Wiley.
909 45. Bateman A, Martin MJ, Orchard S, Magrane M, Agivetova R, Ahmad S, Alpi E,
910 Bowler-Barnett EH, Britto R, Bursteinas B, Bye-A-Jee H, Coetzee R, Cukura A, da
911 Silva A, Denny P, Dogan T, Ebenezer TG, Fan J, Castro LG, Garmiri P,
912 Georghiou G, Gonzales L, Hatton-Ellis E, Hussein A, Ignatchenko A, Insana G,
913 Ishtiaq R, Jokinen P, Joshi V, Jyothi D, Lock A, Lopez R, Luciani A, Luo J, Lussi
914 Y, MacDougall A, Madeira F, Mahmoudy M, Menchi M, Mishra A, Moulang K,
915 Nightingale A, Oliveira CS, Pundir S, Qi G, Raj S, Rice D, Lopez MR, Saidi R,
916 Sampson J, Sawford T, Speretta E, Turner E, Tyagi N, Vasudev P, Volynkin V,
917 Warner K, Watkins X, Zaru R, Zellner H, Bridge A, Poux S, Redaschi N, Aimo L,
918 Argoud-Puy G, Auchincloss A, Axelsen K, Bansal P, Baratin D, Blatter MC,
919 Bolleman J, Boutet E, Breuza L, Casals-Casas C, de Castro E, Echioukh KC,
920 Coudert E, Cuche B, Doche M, Dornevil D, Estreicher A, Famiglietti ML,
921 Feuermann M, Gasteiger E, Gehant S, Gerritsen V, Gos A, Gruaz-Gumowski N,
922 Hinz U, Hulo C, Hyka-Nouspikel N, Jungo F, Keller G, Kerhornou A, Lara V, Le
923 Mercier P, Lieberherr D, Lombardot T, Martin X, Masson P, Morgat A, Neto TB,
924 Paesano S, Pedruzzi I, Pilbout S, Pourcel L, Pozzato M, Pruess M, Rivoire C,
925 Sigrist C, Sonesson K, Stutz A, Sundaram S, Tognolli M, Verbregue L, Wu CH,
926 Arighi CN, Arminski L, Chen C, Chen Y, Garavelli JS, Huang H, Laiho K,
927 McGarvey P, Natale DA, Ross K, Vinayaka CR, Wang Q, Wang Y, Yeh LS,

928 Zhang J, Ruch P, Teodoro D. 2021. UniProt: the universal protein knowledgebase
929 in 2021. Nucleic Acids Res 49:D480–D489.
930 46. Welsh MA, Taguchi A, Schaefer K, Van Tyne D, Lebreton F, Gilmore MS, Kahne
931 D, Walker S. 2017. Identification of a Functionally Unique Family of Penicillin-
932 Binding Proteins. J Am Chem Soc 139:17727–17730.
933 47. Teleman J, Chawade A, Sandin M, Levander F, Malmström J. 2016. Dinosaur: A
934 Refined Open-Source Peptide MS Feature Detector. J Proteome Res 15:2143–
935 2151.
936 48. Ursell T, Lee TK, Shiomi D, Shi H, Tropini C, Monds RD, Colavin A, Billings G,
937 Bhaya-Grossman I, Broxton M, Huang BE, Niki H, Huang KC. 2017. Rapid,
938 precise quantification of bacterial cellular dimensions across a genomic-scale
939 knockout library. BMC Biol 15:1–15.
940 49. Dion MF, Kapoor M, Sun Y, Wilson S, Ryan J, Vigouroux A, van Teeffelen S,
941 Oldenbourg R, Garner EC. 2019. Bacillus subtilis cell diameter is determined by
942 the opposing actions of two distinct cell wall synthetic systems. Nat Microbiol
943 https://doi.org/10.1038/s41564-019-0439-0.
944 50. Van Valen DA, Kudo T, Lane KM, Macklin DN, Quach NT, DeFelice MM, Maayan
945 I, Tanouchi Y, Ashley EA, Covert MW. 2016. Deep Learning Automates the
946 Quantitative Analysis of Individual Cells in Live-Cell Imaging Experiments. PLoS
947 Comput Biol 12:1–24.
948 51. Foster SJ. 1991. Cloning, expression, sequence analysis and biochemical
949 characterization of an autolytic amidase of Bacillus subtilis 168 trpC2. J Gen
950 Microbiol 137:1987–98.

951 52. Foster SJ. 1993. Analysis of Bacillus subtilis 168 prophage-associated lytic
952 enzymes; Identification and characterization of CWLA-related prophage proteins.
953 J Gen Microbiol 139:3177–3184.
954 53. Kuroda A, Sekiguchi J. 1990. Cloning, sequencing and genetic mapping of a
955 Bacillus subtilis cell wall hydrolase gene. J Gen Microbiol 136:2209–2216.
956 54. Nugroho FA, Yamamoto H, Kobayashi Y, Sekiguchi J. 1999. Characterization of a
957 new sigma-K-dependent peptidoglycan hydrolase gene that plays a role in
958 Bacillus subtilis mother cell lysis. J Bacteriol 181:6230–6237.
959 55. Longchamp PF, Mauel C, Karamata D. 1994. Lytic enzymes associated with
960 defective prophages of Bacillus subtilis: Sequencing and characterization of the
961 region comprising the N-acetylmuramoyl-L-alanine amidase gene of prophage
962 PBSX. Microbiology 140:1855–1867.
963 56. Longchamp PF, Mauel C, Karamata D. 1984. Lytic enzymes associated with
964 defective prophages of Bacillus subtilis : sequencing and characterization of the
965 region comprising the N-acetylmuramoyl-L-alanine amidase gene of prophage
966 PBSX.
967 57. Regamey A, Karamata D. 1998. The N-acetylmuramoyl-L-alanine amidase
968 encoded by the Bacillus subtilis 168 prophage SPβ. Microbiology 144:885–893.
969 58. Kuroda A, Asami Y, Sekiguchi J. 1993. Molecular cloning of a sporulation-specific
970 cell wall hydrolase gene of Bacillus subtilis. J Bacteriol 175:6260–6268.
971 59. Smith TJ, Foster SJ. 1995. Characterization of the involvement of two
972 compensatory autolysins in mother cell lysis during sporulation of Bacillus subtilis
973 168. J Bacteriol 177:3855–3862.

974 60. Sekiguchi J, Akeo K, Yamamoto H, Khasanov FK, Alonso JC, Kuroda A. 1995.
975 Nucleotide sequence and regulation of a new putative cell wall hydrolase gene,
976 cwlD, which affects germination in Bacillus subtilis. J Bacteriol 177:5582–5589.
977 61. Atrih A, Zöllner P, Allmaierr G, Foster SJ. 1996. Structural analysis of Bacillus
978 subtilis 168 endospore peptidoglycan and its role during differentiation. J Bacteriol
979 178:6173–6183.
980 62. Popham DL, Helin J, Costello CE, Setlow P. 1996. Muramic lactam in
981 peptidoglycan of Bacillus subtilis spores is required for spore outgrowth but not for
982 spore dehydration or heat resistance. Proc Natl Acad Sci U S A 93:15405–15410.
983 63. Gilmore ME, Bandyopadhyay D, Dean AM, Linnstaedt SD, Popham DL. 2004.
984 Production of Muramic δ-Lactam in Bacillus subtilis Spore Peptidoglycan. J
985 Bacteriol 186:80–89.
986 64. Margot P, Karamata D. 1992. Identification of the structural genes for N-
987 acetylmuramoyl-l-alanine amidase and its modifier in Bacillus subtilis 168:
988 inactivation of these genes by insertional mutagenesis has no effect on growth or
989 cell separation. Mol Gen Genet MGG 232:359–366.
990 65. Lazarevic V, Margot P, Soldo B, Karamata D. 1992. Sequencing and analysis of
991 the Bacillus subtilis lytRABC divergon: a regulatory unit encompassing the
992 structural genes of the N-acetylmuramoyl-L-alanine amidase and its modifier. J
993 Gen Microbiol 138:1949–1961.
994 66. Kuroda A, Sekiguchi J. 1991. Molecular cloning and sequencing of a major
995 Bacillus subtilis autolysin gene. J Bacteriol 173:7304–7312.
996 67. Fischer KE, Bremer E. 2012. Activity of the osmotically regulated yqiHIK promoter

997 from bacillus subtilis is controlled at a distance. J Bacteriol 194:5197–5208.
998 68. Palomino MM, Sanchez-Rivas C, Ruzal SM. 2009. High salt stress in Bacillus
999 subtilis: involvement of PBP4* as a peptidoglycan hydrolase. Res Microbiol
1000 160:117–124.
1001 69. Litzinger S, Duckworth A, Nitzsche K, Risinger C, Wittmann V, Mayer C. 2010.
1002 Muropeptide rescue in Bacillus subtilis involves sequential hydrolysis by β-N-
1003 acetylglucosaminidase and N-acetylmuramyl-L-alanine amidase. J Bacteriol
1004 192:3132–3143.
1005 70. Lambert EA, Sherry N, Popham DL. 2012. In vitro and in vivo analyses of the
1006 Bacillus anthracis spore cortex lytic protein SleL. Microbiology 158:1359–1368.
1007 71. Lambert EA, Popham DL. 2008. The Bacillus anthracis SleL (YaaH) protein is an
1008 N-Acetylglucosaminidase involved in spore cortex depolymerization. J Bacteriol
1009 190:7601–7607.
1010 72. Üstok FI, Chirgadze DY, Christie G. 2015. Structural and functional analysis of
1011 SleL, a peptidoglycan lysin involved in germination of Bacillus spores. Proteins
1012 Struct Funct Bioinforma 83:1787–1799.
1013 73. Margot P, Mauël C, Karamata D. 1994. The gene of the N-acetylglucosaminidase,
1014 a Bacillus subtilis 168 cell wall hydrolase not involved in vegetative cell autolysis.
1015 Mol Microbiol 12:535–545.
1016 74. Rashid MH, Mori M, Sekiguchi J. 1995. Glucosaminidase of Bacillus subtilis:
1017 Cloning, regulation, primary structure and biochemical characterization.
1018 Microbiology 141:2391–2404.
1019 75. Horsburgh GJ, Atrih A, Williamson MP, Foster SJ. 2003. LytG of Bacillus subtilis

1020 is a novel peptidoglycan hydrolase: The major active glucosaminidase.
1021 Biochemistry 42:257–264.
1022 76. Quay DHX, Cole AR, Cryar A, Thalassinos K, Williams MA, Bhakta S, Keep NH.
1023 2015. Structure of the stationary phase survival protein YuiC from B.subtilis. BMC
1024 Struct Biol 15:12.
1025 77. Ishikawa S, Yamane K, Sekiguchi J. 1998. Regulation and characterization of a
1026 newly deduced cell wall hydrolase gene (cwlJ) which affects germination of
1027 Bacillus subtilis spores. J Bacteriol 180:1375–1380.
1028 78. Moriyama R, Fukuoka H, Miyata S, Kudoh S, Hattori A, Kozuka S, Yasuda Y,
1029 Tochikubo K, Makino S. 1999. Expression of a germination-specific amidase,
1030 sleB, of bacilli in the forespore compartment of sporulating cells and its
1031 localization on the exterior side of the cortex in dormant spores. J Bacteriol
1032 181:2373–2378.
1033 79. Boland FM, Atrih A, Chirakkal H, Foster SJ, Moir A. 2000. Complete spore-cortex
1034 hydrolysis during germination of Bacillus subtilis 168 requires SleB and YpeB.
1035 Microbiology 146:57–64.
1036 80. Sudiarta IP, Fukushima T, Sekiguchi J. 2010. Bacillus subtilis CwlQ (previous
1037 YjbJ) is a bifunctional enzyme exhibiting muramidase and soluble-lytic
1038 transglycosylase activities. Biochem Biophys Res Commun 398:606–612.
1039 81. Beachy EH, Keck W, de Pedro MA, Schwarz U. 1981. Exoenzymatic Activity of
1040 Transglycosylase Isolated from Escherichia coli. Eur J Biochem 116:355–358.
1041 82. Sudiarta IP, Fukushima T, Sekiguchi J. 2010. Bacillus subtilis CwlP of the Sp-β
1042 prophage has two novel peptidoglycan hydrolase domains, muramidase and

1043 cross-linkage digesting DD-endopeptidase. J Biol Chem 285:41232–41243.
1044 83. Fukushima T, Kitajima T, Yamaguchi H, Ouyang Q, Furuhata K, Yamamoto H,
1045 Shida T, Sekiguchi J. 2008. Identification and characterization of novel cell wall
1046 hydrolase CwlT: A two-domain autolysin exhibiting N-acetylmuramidase and DL-
1047 endopeptidase activities. J Biol Chem 283:11117–11125.
1048 84. Jorgenson MA, Chen Y, Yahashiri A, Popham DL, Weiss DS. 2014. The bacterial
1049 septal ring protein RlpA is a lytic transglycosylase that contributes to rod shape
1050 and daughter cell separation in Pseudomonas aeruginosa. Mol Microbiol 93:113–
1051 128.
1052 85. Kerff F, Amoroso A, Herman R, Sauvage E, Petrella S, Filée P, Charlier P, Joris
1053 B, Tabuchi A, Nikolaidis N, Cosgrove DJ. 2008. Crystal structure and activity of
1054 Bacillus subtilis YoaJ (EXLX1), a bacterial expansin that promotes root
1055 colonization. Proc Natl Acad Sci U S A 105:16876–16881.
1056 86. Abanes-De Mello A, Sun YL, Aung S, Pogliano K. 2002. A cytoskeleton-like role
1057 for the bacterial cell wall during engulfment of the Bacillus subtilis forespore.
1058 Genes Dev 16:3253–3264.
1059 87. Kuroda A, Rashid MH, Sekiguchi J. 1992. Molecular cloning and sequencing of
1060 the upstream region of the major Bacillus subtilis autolysin gene: a modifier
1061 protein exhibiting sequence homology to the major autolysin and the spoIID
1062 product. J Gen Microbiol 138:1067–1076.
1063 88. Kuroda A, Sekiguchi J. 1992. Characterization of the Bacillus subtilis CwbA
1064 protein which stimulates cell wall lytic amidases. FEMS Microbiol Lett 95:109–
1065 113.

1066 89. Yamaguchi H, Furuhata K, Fukushima T, Yamamoto H, Sekiguchi J. 2004.
1067 Characterization of a new Bacillus subtilis peptidoglycan hydrolase gene, yvcE
1068 (named cwlO), and the enzymatic properties of its encoded protein. J Biosci
1069 Bioeng 98:174–181.
1070 90. Margot P, Wahlen M, Gholamhuseinian A, Piggot P, Karamata D. 1998. The lytE
1071 gene of Bacillus subtilis 168 encodes a cell wall hydrolase. J Bacteriol 180:749–
1072 752.
1073 91. Suzuki T, Tahara Y. 2003. Characterization of the Bacillus subtilis ywtD gene,
1074 whose product is involved in γ-polyglutamic acid degradation. J Bacteriol
1075 185:2379–2382.
1076 92. Fukushima T, Uchida N, Ide M, Kodama T, Sekiguchi J. 2018. DL-
1077 endopeptidases function as both cell wall hydrolases and poly-γ-glutamic acid
1078 hydrolases. Microbiol (United Kingdom) 164:277–286.
1079 93. Schmidt DMZ, Hubbard BK, Gerlt JA. 2001. Evolution of enzymatic activities in
1080 the enolase superfamily: Functional assignment of unknown proteins in bacillus
1081 subtilis and Escherichia coli as L-Ala-D/L-Glu epimerases. Biochemistry
1082 40:15707–15715.
1083 94. Hourdou ML, Guinand M, Vacheron MJ, Michel G, Denoroy L, Duez C, Englebert
1084 S, Joris B, Weber G, Ghuysen JM. 1993. Characterization of the sporulation-
1085 related γ-D-glutamyl-(L)mesodiaminopimelic-acid-hydrolysing peptidase I of
1086 Bacillus sphaericus NCTC 9602 as a member of the metallo(zinc)
1087 carboxypeptidase A family: Modular design of the protein. Biochem J 292:563–
1088 570.

1089 95. Fukushima T, Yao Y, Kitajima T, Yamamoto H, Sekiguchi J. 2007.
1090 Characterization of new L,D-endopeptidase gene product CwlK (previous YcdD)
1091 that hydrolyzes peptidoglycan in Bacillus subtilis. Mol Genet Genomics 278:371–
1092 383.
1093 96. Horsburgh GJ, Atrih A, Foster SJ. 2003. Characterization of LytH, a
1094 differentiation-associated peptidoglycan hydrolase of Bacillus subtilis involved in
1095 endospore cortex maturation. J Bacteriol 185:3813–3820.
1096 97. Pedreira T, Elfmann C, Stülke J. 2022. The current state of SubtiWiki, the
1097 database for the model organism Bacillus subtilis. Nucleic Acids Res 50:D875–
1098 D882.
1099 98. Glauner B, Holtje J V., Schwarz U. 1988. The composition of the murein of
1100 Escherichia coli. J Biol Chem 263:10088–10095.
1101 99. Pasquina-Lemonche L, Burns J, Turner RD, Kumar S, Tank R, Mullin N, Wilson
1102 JS, Chakrabarti B, Bullough PA, Foster SJ, Hobbs JK. 2020. The architecture of
1103 the Gram-positive bacterial cell wall. Nature 582:294–297.
1104

Name (alias)	PY79	UniProt Locus tag	Regulons	e-value	References	Activity
AMIDASE						
Amidase_2 (PF01510)						
cwlA	Y/KO	P24808 BSU25900		5.60E-19	(51–53)	Amidase (51)
cwlH (yqeE)	Y/KO	P54450 BSU25710	gerE^*, sigK^*	7.50E-25	(54)	Amidase (54)
xlyA	Y/KO	P39800 BSU12810	xpf*	1.00E-23	(55)	Amidase (56)
xlyB (yjpB)	Y/KO	O34391 BSU12460		2.20E-18	similarity; xlyA	ND
blyA (yomC)	N	O31982 BSU21410		2.30E-18	(57)	Amidase (57)
Amidase_3 (PF01520)						
cwlC	Y/KO	Q06320 BSU17410	sigK^*	3.4E-44	(58, 59)	Amidase (59)
cwlD	Y/KO	P50864 BSU01530	lexA^*, sigE^*, sigG^*	1.10E-48	(19, 51, 52, 53)	Amidase (63)
lytC (cwlB)	Y/KO	Q02114 BSU35620	sigA^*, sigD^*, sinR^*, slrR^*, yvrHB^*	6.4E-54	(7, 59, 64–66)	Amidase (66)
yqiI	Y/KO	P54525 BSU24190	sigA*	5.50E-56	(67)	SU (67)
yrvJ	Y/KO	O32041 BSU27580	sigH^	2.30E-44	similarity; lytC	ND
Amidase_6 (PF12671)						
yhbB (ygaQ)	Y/KO	O31589 BSU08920	sigE^*	1.50E-39	uncharacterized	ND
yjcM	Y/KO	O31635 BSU11910	abrB*, sigD*	1.30E-23	uncharacterized	ND
SpoIIP (PF07454)						
spoIIP	Y/KO	P37968 BSU25530	sigE^*, sigF^*, sigG^*, spoVT^*	9.70E-79	(24, 25)	amidase, DDEP (25)
Beta-lactamase (PF00144)						
pbpE	Y/KO	P32959 BSU34440	sigW^*	3.40E-61	(68)	SU (68)
pbpX	Y/KO	O31773 BSU16950	sigM^*, sigV^*, sigW^, sigX^*	7.90E-54	similarity; pbpE	ND
amiE (ybbE)	Y	O05213 BSU01670	murR*	7.40E-76	does not hydrolyse PG (69)	
N-ACETYLGLUCOSAMIDASE/LYTIC TRANSGLYCOSYLASE						
Glyco_hydro_3 (PF01915)						
nagZ (yzbA, ybbD)	Y	P40406 BSU01660	murR*	6.50E-131	does not hydrolyse PG (69)	
Glyco_hydro_18 (PF00704)						
yaaH (sleL)	Y/KO	P37531 BSU00160	sigB^*, sigE^*, spoIIID^*	1.20E-26	cleaves small fragments (70–72)	Glucosaminidase (B. anthracis SleL,(71))
ydhD	Y/KO	O05495 BSU05710	sigE^*	9.60E-30	similarity; yaaH	ND
ykvQ	Y/KO	O31682 BSU13790	sigK^*	2.50E-23	similarity; yaaH	ND
yvbX	Y/KO	O32258 BSU34020		1.10E-33	similarity; yaaH	ND

				Glucosaminidase (PF01832)			
lytD (cwlG)	Y/KO	P39848	BSU35780	sigD^*, sigG^	3.30E-11	(7, 73, 74)	Glucosaminidase (73)
lytG	Y/KO	O32083	BSU31120		6.80E-24	(75)	Glucosaminidase (75)
				3D (PF06725)			
yabE	Y/KO	P37546	BSU00400	sigA*	1.80E-22	similarity; yuiC, yocH	ND
yocH	Y/KO	O34669	BSU19210	abrB^*, sigA^*, spo0A^*, walR^*	3.50E-22	(35)	SU (35)
yuiC	Y/KO	O32108	BSU32070	codY^*, sigF^*	9.40E-21	(76)	LTG (76)
yorM	N	O31901	BSU20330		7.90E-11	similarity; yuiC, yocH	ND
				Hydrolase_2 (PF07486)			
cwlJ (ycbQ)	Y/KO	P42249	BSU02600	sigE^*, sigK^*, spoIIID^*	1.60E-18	(77)	ND
sleB (ypeA)	Y/KO	P50739	BSU22930	sigG^*	1.20E-25	(23, 78, 79)	LTG (79)
ykvT	Y/KO	O31685	BSU13820	walR*	5.80E-28	similarity; sleB, cwlJ	ND
				SLT (PF01464)			
xkdO	Y/KO	P54334	BSU12680	xpf*	6.20E-20	similarity; cwlQ, cwlP	ND
cwlQ (yjbJ)	Y/KO	O31608	BSU11570	sigD^*	1.70E-34	(80, 81)	LTG + muramidase (80)
yqbO	Y/KO	P45931	BSU26030		5.70E-24	similarity; cwlQ, cwlP	ND
cwlP (yomI)	Y/KO	O31976	BSU21350		1.80E-32	(82)	Muramidase** (82)
				Lysozyme_like (PF13702)			
yocA	Y/KO	O34636	BSU19130		4.30E-59	similarity; CwlT	ND
cwlT (yddH)	N	P96645	BSU04970	immR*	2.10E-42	(83)	Muramidase** (83)
				DPBB_1 (PF03330)			
ydjM (yzvA)	Y/KO	P40775	BSU06250	phoP*, walR*	1.00E-09	similarity; PaRlpA (84)	ND
yoaJ (EXLX1)	N	O34918	BSU18630	fur*	2.90E-07	does not hydrolyse PG (85)	
				SpoIID (PF08486)			
spoIID (spoIIC)	Y/KO	P07372	BSU36750	sigE^*, spoIIID^*	1.30E-23	(25, 86)	LTG (25)
lytB (cwbA)	Y	Q02113	BSU35630	sigA^*, sigD^*, sinR^*, slrR^*, yvrHB^*	3.90E-23	does not hydrolyse PG (87, 88)	
				YceG (PF02618)			
mltG (yrrL)	Y	O34758	BSU27370	spo0A^*	3.20E-90	similarity; EcMltG (16); membrane bound	LTG (17-18)
sweC (yqzC)	Y	O32023	BSU24940	spo0A^*	1.40E-07	similarity; EcMltG (16); membrane bound	ND
				PEPTIDASE			
				DL-endopeptidase			

				NLPC/P60 (PF00877)			
cwlO (yzkA,yvcE)	Y	P40767	BSU34800	sigA*, walR*	4.40E-29	(89)	DLEP (89)
cwlS (yojL)	Y/KO	O31852	BSU19410	abh^*, abrB^*, ccpA^*, sigD^*, sigH^*	4.70E-29	(11)	DLEP (11)
lytE (papQ, cwlF)	Y	P54421	BSU09420	sigA^*, sigH^*, sigI^*, spo0A^*, walR^*	3.30E-28	(22, 90)	SU (22)
lytF (cwlE, ydhD)	Y/KO	O07532	BSU09370	sigD^*, sinR^*, slrR^*	1.40E-28	(20, 21)	DLEP (21)
pgdS (ywtD)	Y	P96740	BSU35860	sigD^*	1.00E-22	does not hydrolyze PG (91, 92)	
ykfC	Y/KO	O35010	BSU12990	codY*	1.80E-29	(93)	DLEP (93)
cwlT (yddH)	N	P96645	BSU04970	immR*	3.50E-34	(83)	DLEP** (83)
				Peptidase_M14 (PF00246)			
yqgT	Y/KO	P54497	BSU24830		2.70E-27	similarity to B. sphaericus EP1, (94)	ND
				Peptidase_C92 (PF05708)			
yycO	Y/KO	Q45607	BSU40280	sigK^*	5.0E-5		ND
				LD-endopeptidase			
				Peptidase_M15 (PF01427)			
cwlK (ycdD)	Y/KO	O34360	BSU02810		3.10E-20	(95)	LDEP (95)
				Peptidase_M23 **(**PF01551**)**			
lytH (yunA, yutA)	Y/KO	O32130	BSU32340	sigK^*	1.80E-21	(96)	LDEP (96)
spoIIQ	Y	P71044	BSU36550	sigF^*	1.00E-24	membrane bound	ND
spoIVFA	Y	P26936	BSU27980	sigE^*, spoIIID^*	3.40E-12	membrane bound	ND
cwlP (yomI)	N	O31976	BSU21350		1.80E-27	(82)	DDEP** (82)

WT
ΔcwlO
ΔlytE
ΔcwlQ
ΔyocH
ΔlytD
LO
ΔlytC
ΔykvT
ΔpbpX
ΔypbE
LO
ΔpbpE
ΔxlyB
ΔpbpX
ΔlytG
LO
ΔcwlA
ΔykfC
ΔyqgT
ΔyqiL
LO
ΔcwlK
ΔyrvJ
ΔxlyA
ΔcwlC
LO
ΔcwlD
ΔsleB
ΔcwlJ
ΔlytH
LO
ΔcwlH
ΔydhD
ΔyaaH
ΔcwlS
LO
ΔyqgT
ΔcwlC
ΔydjM
ΔxkdO
LO
ΔyabE
ΔyqbO
LO
ΔyuiC
ΔyocA
LO
ΔlytF
LO
ΔspoIID
ΔspoIIP
LO
ΔykvQ
ΔyvbX
ΔyhbB
LO
ΔyjcM
Δ40
Δ40ΔcwlO
Δ40ΔlytE
ΔyycO, LO

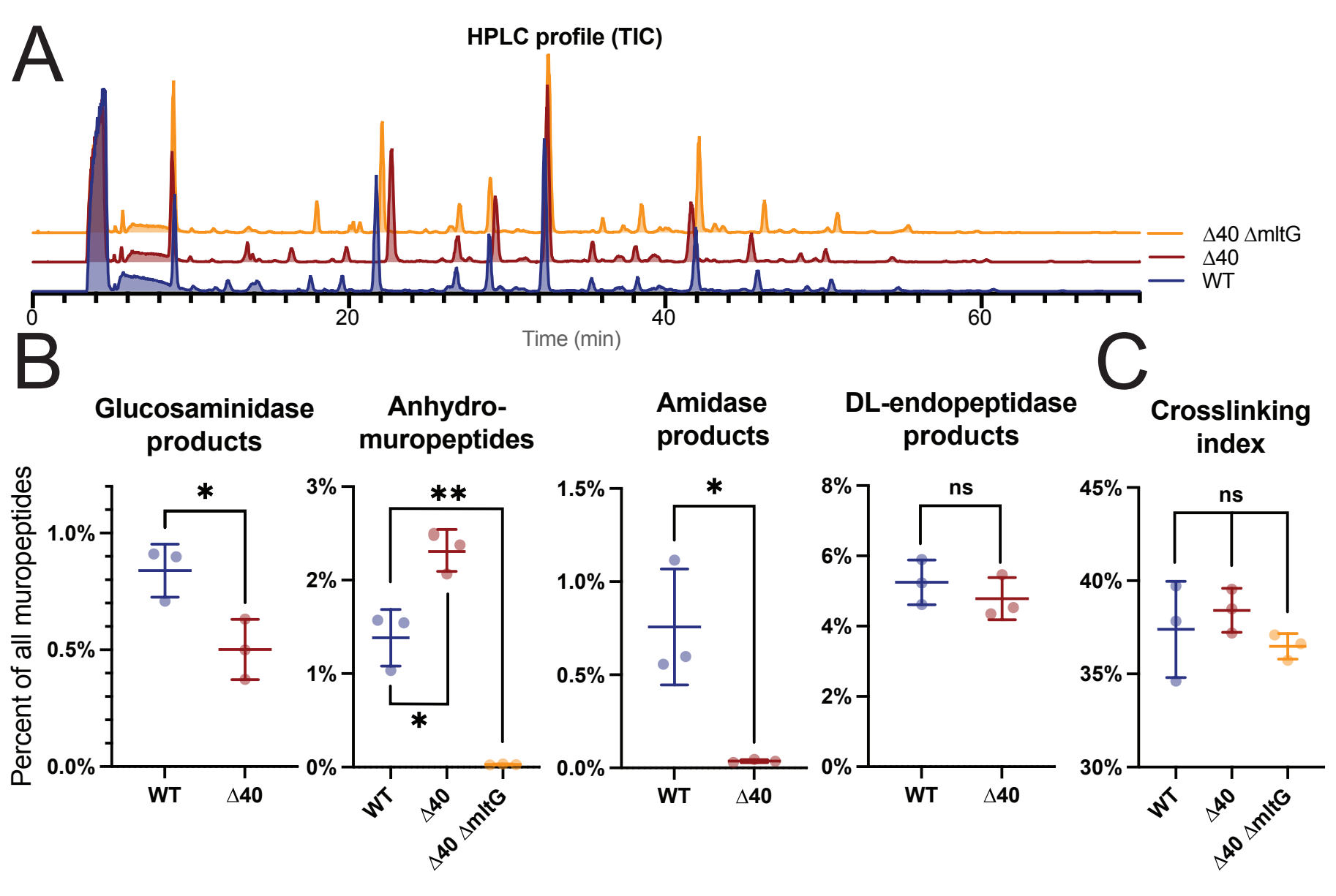
A
HPLC profile (TIC)
Δ40 ΔmltG
Δ40
WT
0
20
40
60
Time (min)
B
Glucosaminidase products
Anhydro-muropeptides
Amidase products
DL-endopeptidase products
C
Crosslinking index
Percent of all muropeptides
1.0%
0.5%
0.0%
3%
2%
1%
0%
1.5%
1.0%
0.5%
0.0%
8%
6%
4%
2%
0%
45%
40%
35%
30%
*
**
*
*
ns
ns
WT
Δ40
Δ40 ΔmltG

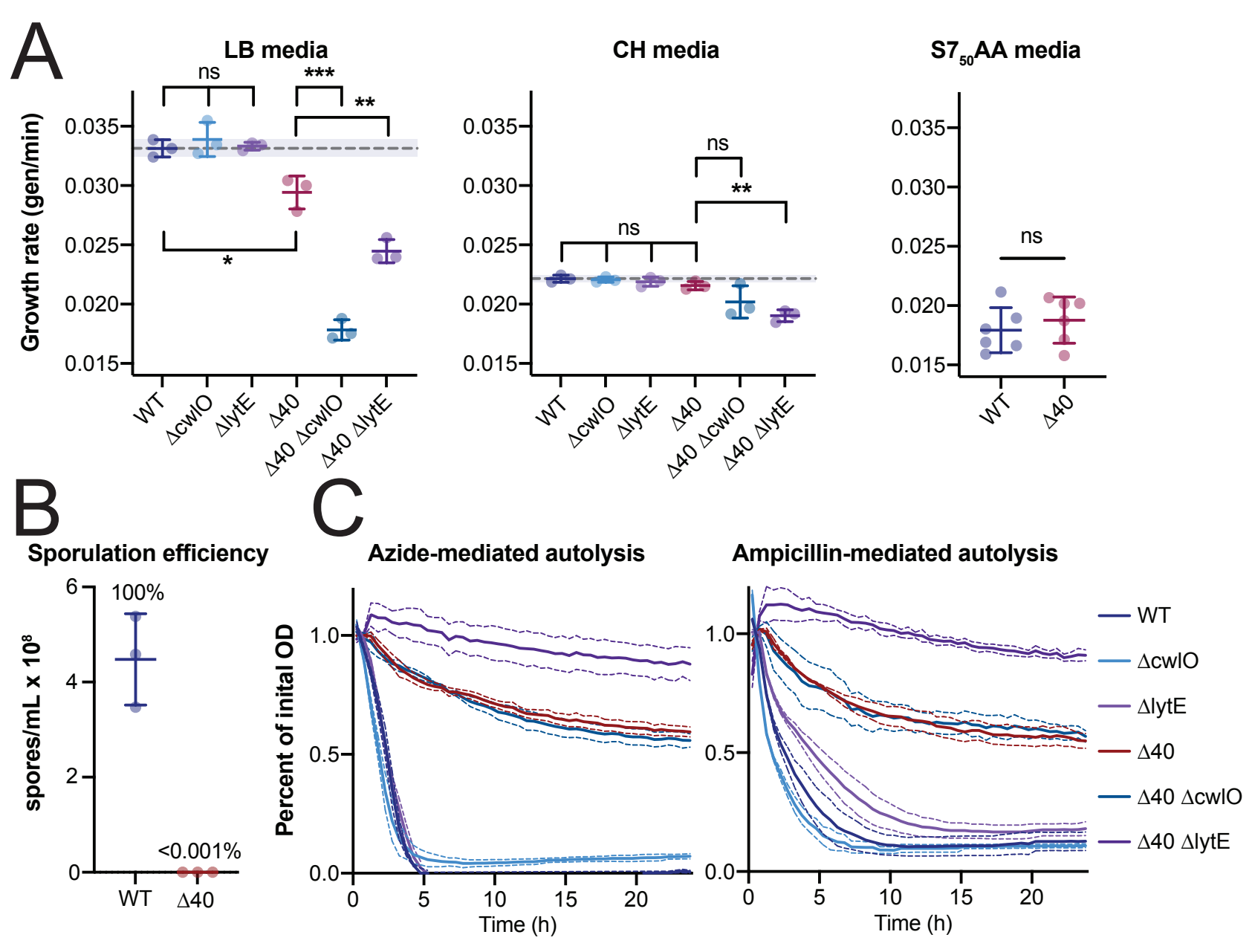
A
LB media
CH media
S7$_{50}$AA media
Growth rate (gen/min)
0.035
0.030
0.025
0.020
0.015
ns
***
**
*
WT
ΔcwlO
ΔlytE
Δ40
Δ40 ΔcwlO
Δ40 ΔlytE
B
Sporulation efficiency
spores/mL x 10^8
6
4
2
0
100%
<0.001%
C
Azide-mediated autolysis
Ampicillin-mediated autolysis
Percent of inital OD
1.0
0.5
0.0
0
5
10
15
20
Time (h)

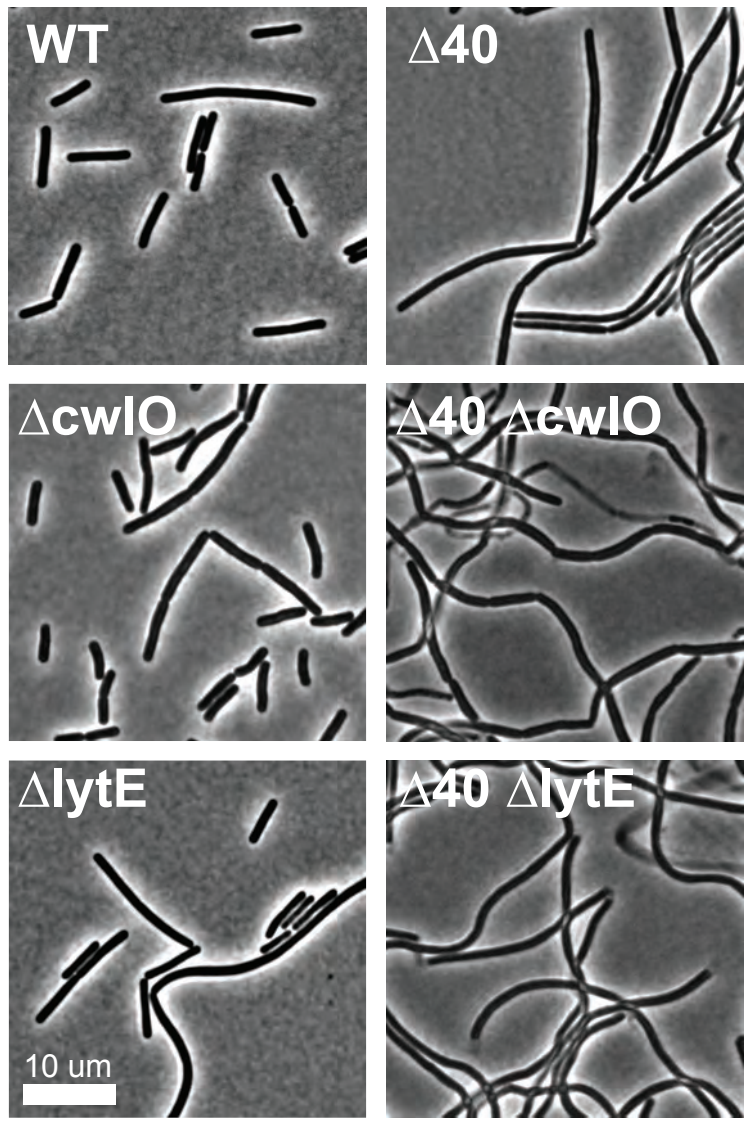
A
WT
Δ40
ΔcwlO
Δ40 ΔcwlO
ΔlytE
Δ40 ΔlytE
10 um

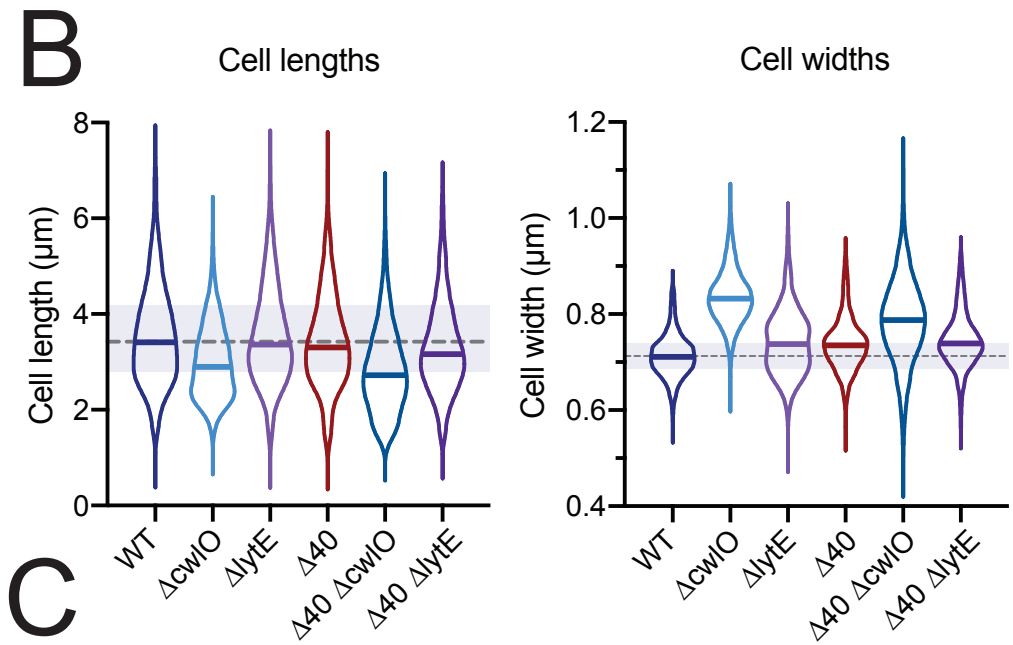
B
Cell lengths
Cell length (µm)
0
2
4
6
8
WT
ΔcwlO
ΔlytE
Δ40
Δ40 ΔcwlO
Δ40 ΔlytE
Cell widths
Cell width (µm)
0.4
0.6
0.8
1.0
1.2
WT
ΔcwlO
ΔlytE
Δ40
Δ40 ΔcwlO
Δ40 ΔlytE

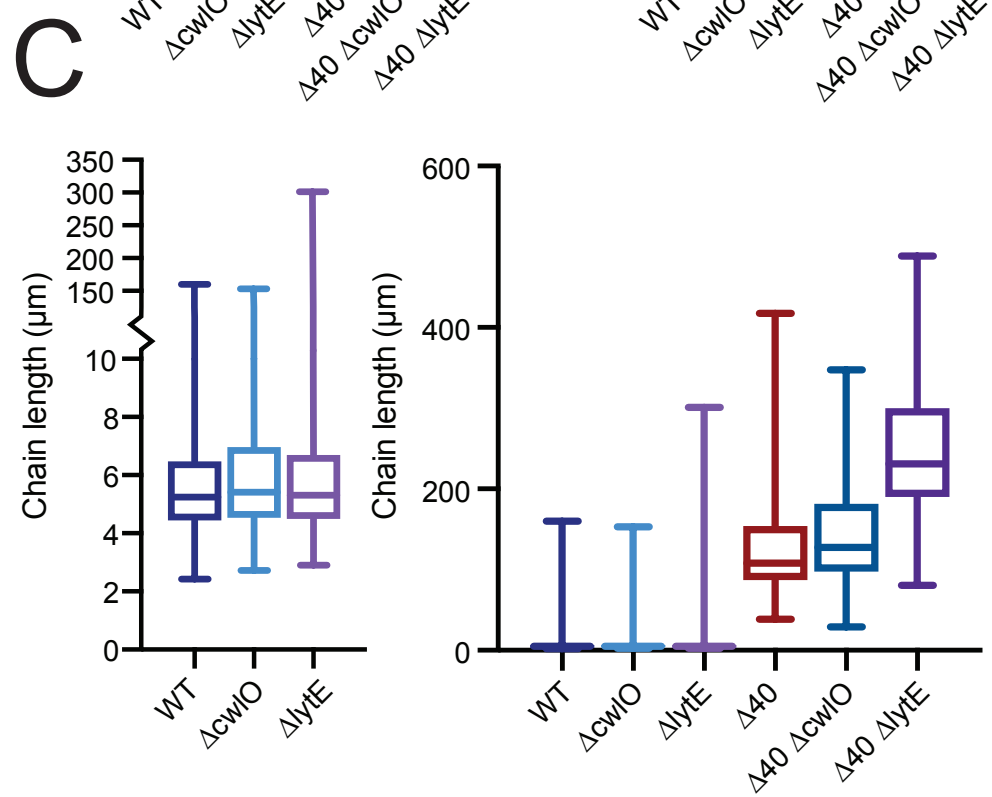
C
Chain length (µm)
0
2
4
6
8
10
150
200
250
300
350
WT
ΔcwlO
ΔlytE
Chain length (µm)
0
200
400
600
WT
ΔcwlO
ΔlytE
Δ40
Δ40 ΔcwlO
Δ40 ΔlytE

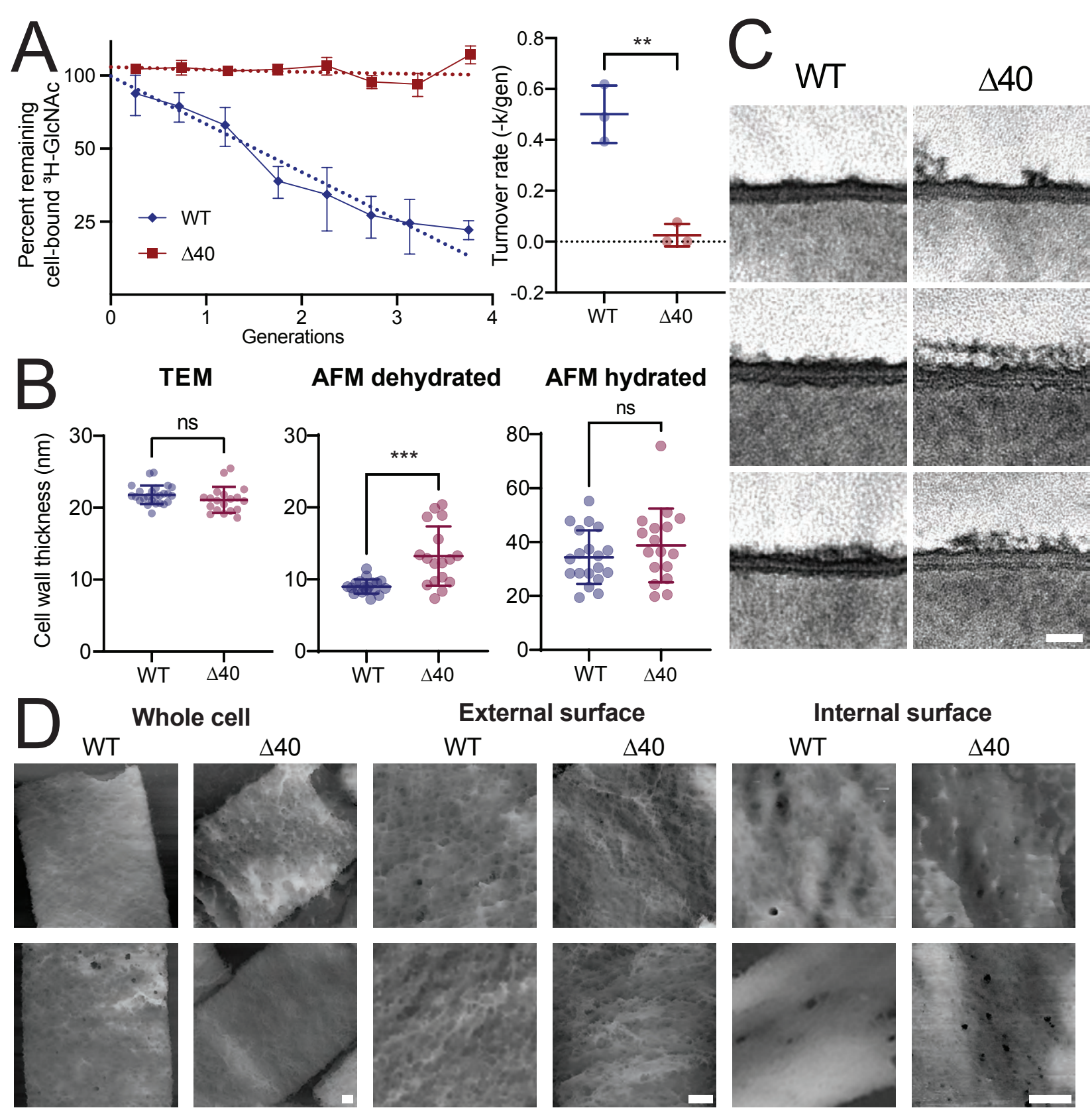
A
Percent remaining cell-bound ³H-GlcNAc
100
50
25
WT
Δ40
0
1
2
3
4
Generations
Turnover rate (-k/gen)
0.8
0.6
0.4
0.2
0.0
-0.2
**
WT
Δ40
B
TEM
AFM dehydrated
AFM hydrated
Cell wall thickness (nm)
ns
***
ns
30
20
10
0
80
60
40
20
WT
Δ40
C
WT
Δ40
D
Whole cell
External surface
Internal surface
WT
Δ40
WT
Δ40
WT
Δ40

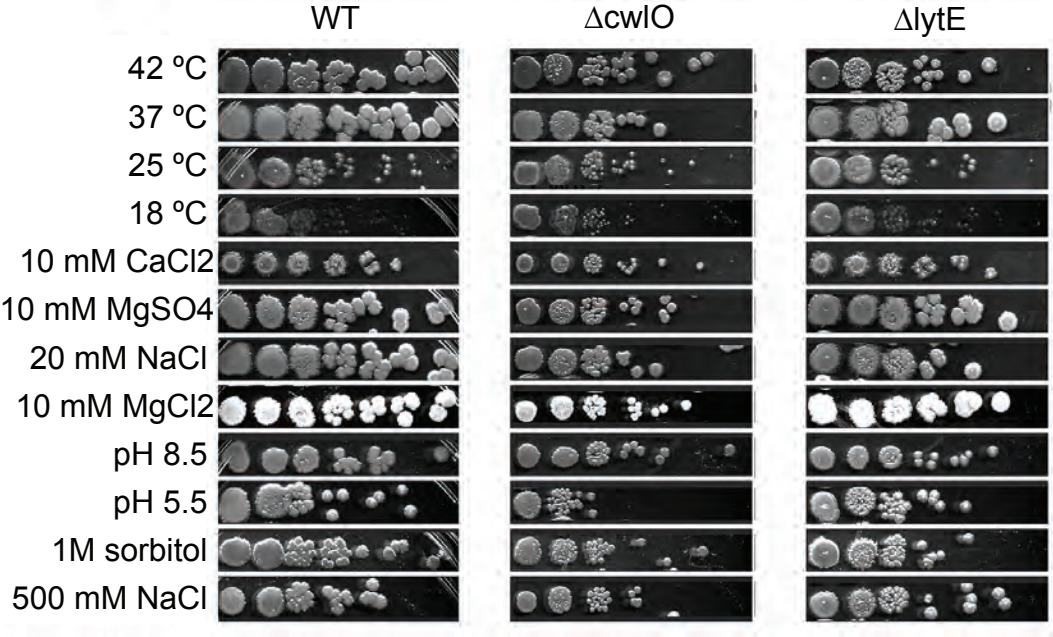
WT
ΔcwlO
ΔlytE
42 ºC
37 ºC
25 ºC
18 ºC
10 mM CaCl2
10 mM MgSO4
20 mM NaCl
10 mM MgCl2
pH 8.5
pH 5.5
1M sorbitol
500 mM NaCl

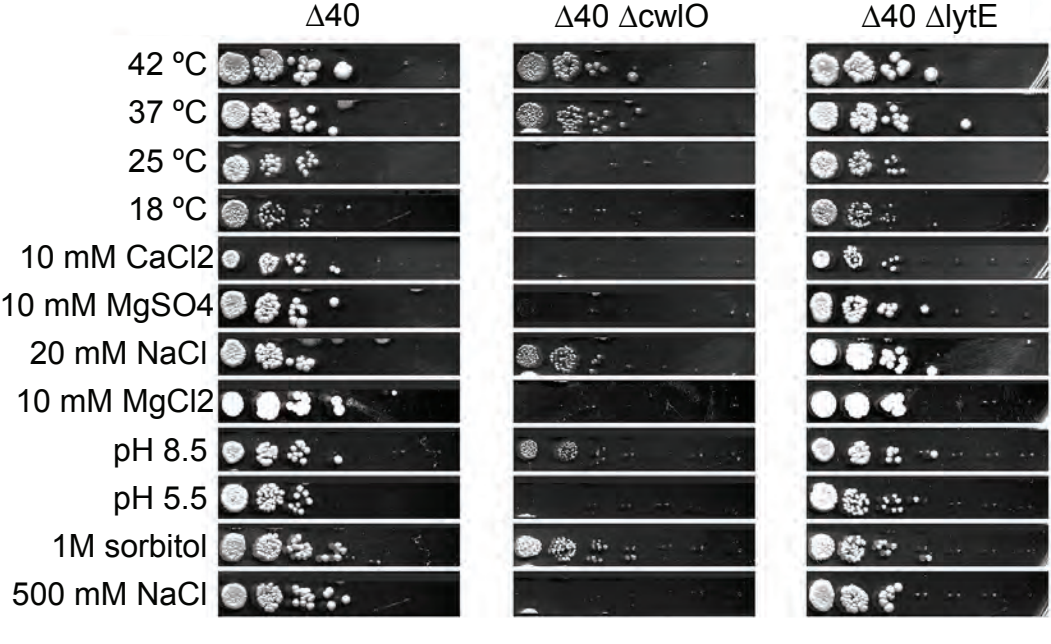
Δ40
Δ40 ΔcwlO
Δ40 ΔlytE
42 ºC
37 ºC
25 ºC
18 ºC
10 mM CaCl2
10 mM MgSO4
20 mM NaCl
10 mM MgCl2
pH 8.5
pH 5.5
1M sorbitol
500 mM NaCl

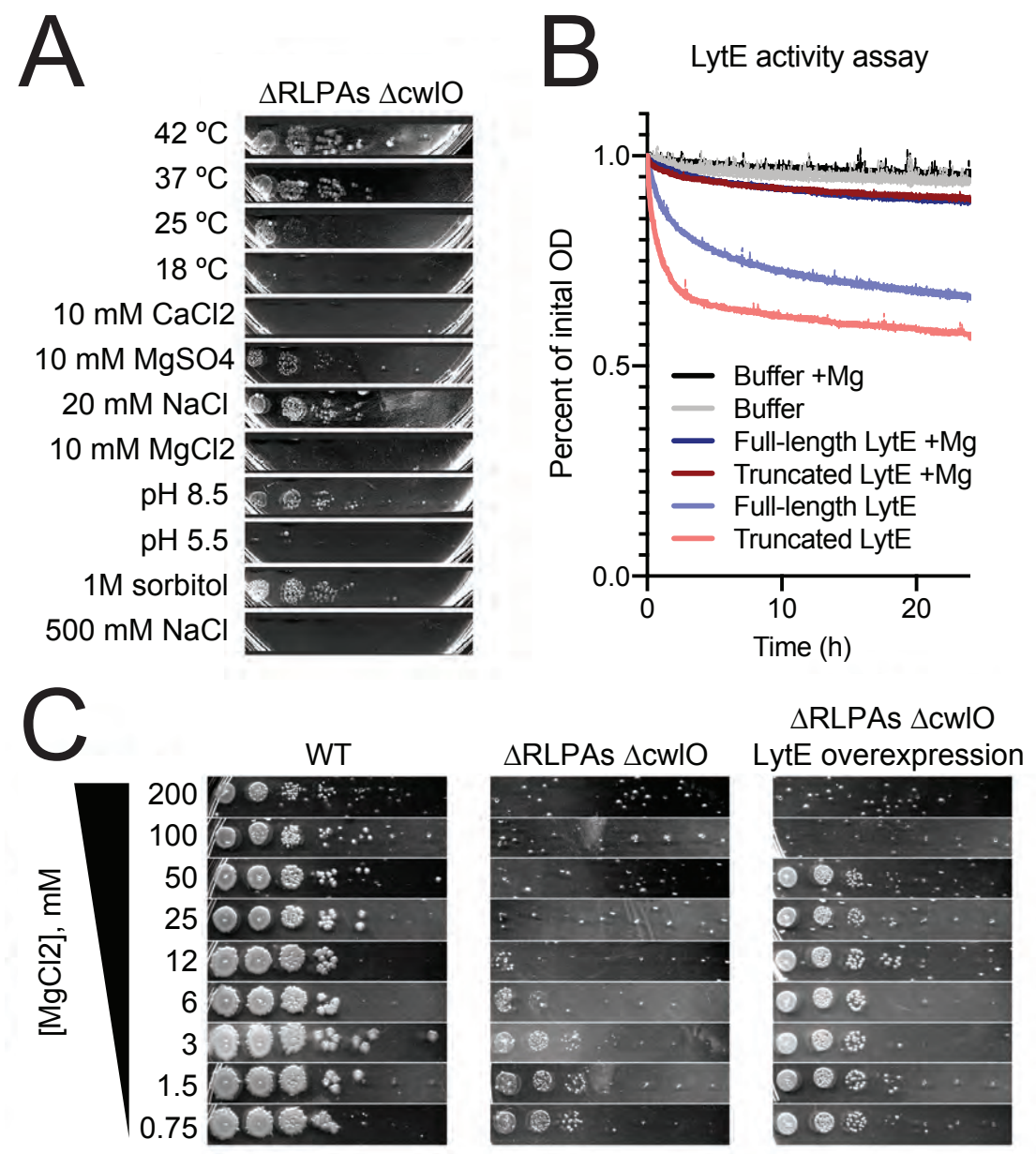
A
ΔRLPAs ΔcwlO
42 ºC
37 ºC
25 ºC
18 ºC
10 mM CaCl2
10 mM MgSO4
20 mM NaCl
10 mM MgCl2
pH 8.5
pH 5.5
1M sorbitol
500 mM NaCl
B
LytE activity assay
Percent of inital OD
1.0
0.5
0.0
0
10
20
Time (h)
Buffer +Mg
Buffer
Full-length LytE +Mg
Truncated LytE +Mg
Full-length LytE
Truncated LytE
C
WT
ΔRLPAs ΔcwlO
ΔRLPAs ΔcwlO
LytE overexpression
[MgCl2], mM
200
100
50
25
12
6
3
1.5
0.75